Latin American Journal of Solids and Structures
www.lajss.org

On the Nonlinear Transient Analysis of Planar Steel Frames with Semi-Rigid Connections: From Fundamentals to Algorithms and Numerical Studies

Abstract

This paper presents the fundamentals for prediction of a more realistic behavior of planar steel frames with semi-rigid connections under dynamic loading. The majority of the research in this area concentrates on the nonlinear static analysis of frames with semi-rigid connections. Indeed, few studies have contributed to the nonlinear dynamic and vibration analyses of frames. Therefore, this article first describes the frames' semi-rigid connection behavior under monotonic and cyclic loads, and presents the independent hardening technique adopted to simulate the joint behavior under cyclic excitation. In a finite element context, this paper presents an efficient numerical methodology that is proposed in algorithmic form to obtain the nonlinear transient response of the structural system. The paper also presents, in algorithmic form, a complete description of the adopted connection hysteretic model. Satisfying the equilibrium and compatibility conditions, and assuming only the connection's rotational deformation due to bending as variable, this work obtains the tangent stiffness and mass matrices of the beam-column element with semi-rigid connections at the ends. The study concludes by verifying and validating the proposed numerical approach using four structural steel systems: a L-frame, a two-story frame, a six-story frame, and a four-bay five-story frame. The analyses show that the hysteresis of the semi-rigid connection has a strong effect on the frames' responses and is an important source of damping during the structural vibration.

Keywords

Steel frames, Nonlinear transient analysis, Geometric nonlinearities, Semi-rigid connections, Connection stiffness, Connection hysteretic behavior.

Andréa R. D. Silva [a]*
Everton A. P. Batelo [a]
Ricardo A. M. Silveira [a]
Francisco A. Neves [a]
Paulo B. Gonçalves [b]

[a] Departamento de Engenharia Civil, Escola de Minas, Universidade Federal de Ouro Preto, Minas Gerais, Brasil. E-mail: andreadiassilva@yahoo.com.br, everton.batelo@gmail.com, ricardo@em.ufop.br, fassis@em.ufop.br

[b] Departamento de Engenharia Civil, Pontifícia Universidade Católica do Rio de Janeiro, Rio de Janeiro, RJ, Brasil. E-mail: paulo@puc-rio.br

*Corresponding author

http://dx.doi.org/10.1590/1679-78254087

Received: June 05, 2017
In Revised Form: October 22, 2017
Accepted: February 27, 2018
Available online: March 20, 2018

1 INTRODUCTION

In the structural design and construction of reticulated steel structures involving one or more floors, the beam-column and column-base connections play a significant role in their structural response. They also represent a significant fraction of the total cost of the structure. Thus, the characteristics of these connections are, in steel structures, economically and structurally significant. Therefore, the engineer must have a good understanding of the connection behavior. In most cases it is advisable to use semi-rigid connections. In fact, modern standards (ABNT - NBR 8800, 2008; AISC, 2010; Eurocode 3, 2005) already include procedures to define the stiffness as well as strength of semi-rigid connections for computational analysis programs and prescriptions for the design engineer.

Various studies on the static analysis of steel frames (King, 1994; Li *et al.*, 1995; Kruger *et al.*, 1995; Chen, 2000; Chan and Chui, 2000; Sekulovic and Nefovska-Danilovic, 2004; Cabrero and Bayo, 2005; Ihaddoudène *et al.*, 2009; Valipour and Bradford, 2012) have already shown that the deformation and bending moment transmission capacity of the connections can significantly alter the load carrying capacity, the internal force distribution and global and local instability of these structures. In addition, within the civil, naval, oceanic, and aeronautical industries, more resistant materials and new design and construction techniques have led to lighter and slender structures, which are, however, usually susceptible to excessive vibration problems. Consequently, an essential part of

a structural design should include an analysis of their dynamic behavior under various loading conditions. Research along these lines, accounting for the effect of connection flexibility, is still limited, particularly compared to the amount of research on static analysis. Numerical investigations into the behavior of steel structures with semi-rigid connections submitted to dynamic situations have been carried out by, among others, the following researchers: Valipour and Bradford (2012); Chan and Ho (1994); Lui and Lopes (1997); Xu and Zhang (2001); Sophianopoulos (2003); Silva *et al*. (2008); Galvão *et al*. (2010); Vimonsatit *et al.* (2012); Nguyen and Kim (2013) Attarnejad and Pirmoz (2014); and Aristizabal-Ochoa (2015).

Researchers have also experimentally evaluated the cyclic responses of semi-rigid connections. Bernuzzi *et al*. (1996), Calado (2003), and Shi *et al*. (2007) carried out tests using specific types of connections and proposed mathematical models to represent the observed behavior.

This article can be considered as an expansion of an earlier work by Galvão *et al*. (2010). In this context, the current paper evaluates, using the CS-ASA Program (Computational System for Advanced Structural Analysis; Silva, 2009), the nonlinear dynamic response of planar steel frame, considering geometric nonlinear effects and the semi-rigid characteristics of the connections between the structural elements. When the semi-rigid connections are submitted to alternating repetitive actions, they may develop an inelastic behavior that gives rise to hysteretic damping, which is in most cases quite beneficial.

CS-ASA is a FEM-based computer system implemented in Fortran 90/95, originally designed for steel structures. This program can perform advanced static and dynamic numerical analysis considering sources of nonlinearities such as second order effects and semi-rigid connections (using pseudo-springs at the finite element ends). Therefore, this paper brings the numerical results obtained from an alterated CS-ASA version, which allow represent the semi-rigid connection hysteretic behavior, in order to allow a better modeling of the nonlinear transient response of planar steel frames with flexible joints. Actually, this is an extension of the CS-ASA initial module that contemplated the static nonlinear analysis and some cases for dynamic nonlinear analysis and vibration (Galvão *et al*., 2010; Silva, 2009). As main contribution, in a finite element context, this paper presents an efficient numerical methodology to obtain the nonlinear transient response of structural systems with semi-rigid joints. The paper also presents, in algorithm form, a complete description of the adopted connection hysteretic behavior.

The next section, Section 2, describes the connection behavior when subjected to monotonic and cyclical loads, and presents the adopted technique to simulate this behavior. Section 3 details the methodology used to obtain the nonlinear transient response of the structural system. Section 4 presents the formulation of the finite element used in the structural system's modeling. Finally, to validate the proposed analysis methodology, Section 5 evaluates the dynamic response of four structural systems. The results demonstrate that the structural dynamic behavior can be greatly influenced by the effects of the semi-rigid connections and that a careful dynamic connection description and dynamic analysis is essential for a safe and yet cost-effective design.

2 SEMI-RIGID CONNECTIONS

As noted above, connections play a key role in the assembly, performance, and cost of a steel structure. In most cases, these connections cannot be modeled as perfectly rigid or ideally hinged. Rigid connections prevent any alteration of the angle between the interlinked elements, transferring the full moment from one extremity to the other. In the case of hinged connections, no moment is transmitted between the elements. These hypotheses simplify the analysis but fail to represent the true behavior of most structures. The experimental investigations of Jones *et al*. (1980; 1983) and Nethercot *et al*. (1998) demonstrated that a greater part of the connections used in current practices display semi-rigid behavior. This can substantially influence the overall stability of the structural system as well as the distribution of the forces acting on its elements. Indeed, geometric and mechanical discontinuities can, according to Colson (1991), introduce localized effects and imperfections in the connections used in steel structures, which interfere with the overall behavior of the structure, providing justification for a more rigorous investigation into these connection behavior. Such studies should take into account not only the manufacturing and assembly point of view but also the connections' influence on the structural response.

Not only the axial and shear forces but also the bending and torsion moments are transmitted through a connection. For a great majority of steel structures, however, the effects of these axial and shear forces on the deformation of the connection are small compared to those caused by the bending moment (Chen *et al*., 1996). For this reason, and knowing that in the analysis of planar structures the deformation caused by torsion is negligible, this study considers only the rotational deformation of the connection caused by bending.

Connection behavior is generally described by moment-rotation curves, which can be obtained in three ways: from experimental tests, numerical simulation in finite elements, or by theoretical models. These latter are developed by applying curve-adjustment techniques to the results obtained by the numerical simulation and/or the

experimental tests. Díaz *et al.* (2011) presented the main features of different connection models, highlighting the advantages and disadvantages of each one. Other studies have been performed to evaluate the behavior of connections under monotonic and cyclic loads, including (Ackroyd and Gerstle, 1982; Azizinamini *et al.*, 1987; Yee and Melchers, 1986; Kishi and Chen, 1987a; Kishi and Chen, 1987b; Korol *et al.*, 1990; Tsai and Popov, 1990; Abolmaali *et al.*, 2003; Abolmaali *et al.*, 2009). The following two subsections describe these behaviors as well as the numerical models adopted here.

2.1 Behavior under Monotonic Loading and Mathematical Representation

Figure 1 illustrates the typical behavior of three types of semi-rigid connections: the flush end plate, top and seat angle, and single web angle. In the figure the relative rotation between the interconnected elements, ϕ_c, due to an applied moment is also shown. These connections, when submitted to bending, display a softening nonlinear behavior with decreasing stiffness. The moment-rotation curve is initially practically linear, but, as the load increases, the nonlinearity increases. This change in behavior is influenced by the existence of stress concentration, geometric imperfections and discontinuities and the plastic behavior of its components. At a certain loading level, these factors begin to interfere in the rotational capacity of the connection. In the final loading stage, the moment-rotation curve tends toward an asymptotical value known as the ultimate moment capacity of connection.

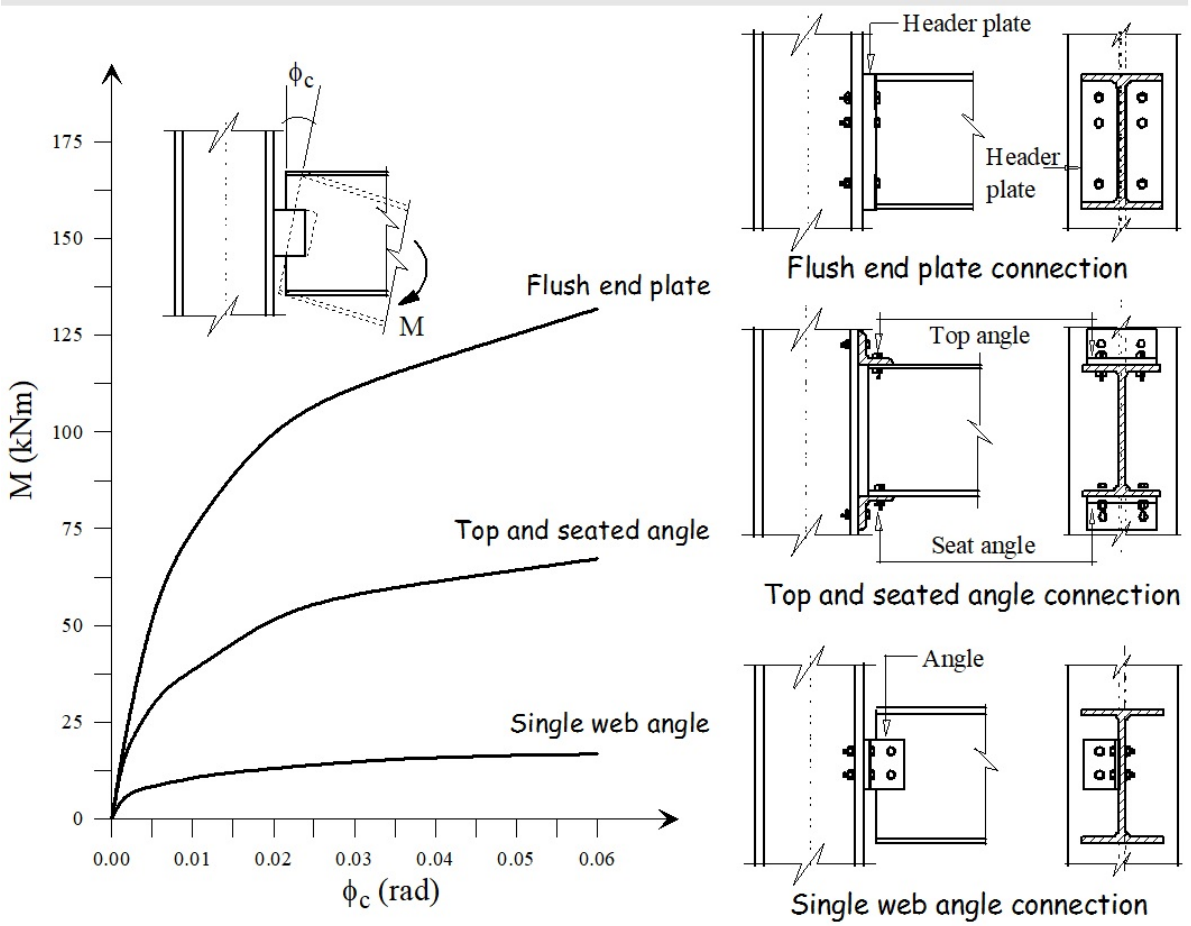

Figure 1: *Moment-rotation curves of three usual types of connections under monotonic loading.*

The most important characteristics that define the connection behavior are its initial stiffness and its ultimate moment capacity (Bjorhovde *et al.*, 1990). The connection stiffness, denoted as S_c, is determined by experimental tests. Mathematically, it represents the inclination of the tangent to the moment-rotation curve (Fig. 1). The stiffness value does not determine whether a connection will behave in a rigid or flexible manner. This behavior can only be established by using a parameter that relates the connection's stiffness to the bending stiffness (*EI*) of the element to which it is connected. Cunningham (1990) proposed, to provide a better understanding of the rotational behavior of the connection, a fixed factor, $\gamma = (1 + 3EI \,/\, (S_c L))^{-1}$, in which L represents the ele-

ment's length, where γ varies between 0 and 1. For a perfectly hinged connection $\gamma = 0$ and for an ideally rigid connection, $\gamma = 1$, since $S_c \to \infty$. The connection stiffness can be calculated by:

$$S_c = \frac{dM}{d\phi_c} \tag{1}$$

where M is the bending moment acting on the connection and ϕ_c is its rotational deformation.

The moment-rotation curves can generally be written by one of the following expressions:

$$\begin{aligned} M &= f(\phi_c) \\ \phi_c &= g(M) \end{aligned} \tag{2}$$

which relate the moment to the rotation with mathematical expressions *f* and *g*, which usually depend on the geometry and disposition of the connecting components and the curve adjustment parameters.

According to Chan and Chui (2000), the mathematical models should provide a smooth moment-rotation curve with the first derivative positive and be able to represent various types of connections. For a linear connection model only one parameter defining the joint stiffness is necessary. In this case, the moment-rotation relationship is given by:

$$M = S_{cini}\ \phi_c \tag{3}$$

where S_{cini} represents the initial stiffness. This is the simplest model and has been widely used in the analysis of semi-rigid connections (Arbabi, 1982; Kawashima and Fujimoto, 1984; Chan, 1994; Lui and Chen, 1986). For large displacement analyses, however, it may lead to erroneous conclusions.

Unlike the linear model, the nonlinear models simulate the stiffness degradation as the load increases. Among the various nonlinear models found in literature, only those employed in this study are discussed.

The first is an exponential model (Lui and Chen, 1986; Chen and Lui, 1991), whose mathematical expression for the moment-rotation curve is given by:

$$M = M_0 + \sum_{m=1}^{n} C_j \left[1 - \exp\left(\frac{-\left|\phi_c\right|}{2m\alpha}\right)\right] + R_p \left|\phi_c\right| \tag{4}$$

where M is the moment in the connection, M_0 is the initial moment, R_p is the strain-hardening stiffness of the connection, α is an scaling factor, and C_m — $m = 1,2,...n$ — is the curve-fitting coefficient.

Also used here is a four-parameter model proposed by Richard and Abbott (1975). The model describes the connection behavior according to the relationship:

$$M = \frac{\left(S_{cini} - R_p\right)\left|\phi_c\right|}{\left[1 + \left|\left(S_{cini} - R_p\right)\left|\phi_c\right| / M_0\right|^n\right]^{1/n}} + R_p \left|\phi_c\right| \tag{5}$$

in which R_p is the strain-hardening stiffness when ϕ_c tends to infinity; n is a parameter that defines the sharpness of the curve, and M_0 is a reference moment. A study made by Kishi *et al.* (2004) demonstrated that this model is effective in establishing the behavior of an end plate connection. However, it can be applied to any type of connection. To do this, it is sufficient to either experimentally or numerically evaluate the four necessary parameters. From this model, three others can be obtained: linear ($R_p \approx S_{cini}$), bilinear ($n \to \infty$), and ignoring the effect of the strain-hardening stiffness, the three-parameter potential model presented by Kishi and Chen (1986). The stiffness of the connection is obtained using Eq. (1), with M described by one of the nonlinear presented models.

2.2 Behavior under Cyclic Loading and Mathematical Representation

When a realistic numerical simulation of a given structural system under dynamic loads is desired, it is essential to consider the behavior of the connection under cyclic load. Depending on the load level and time history, semi-rigid connections may develop an inelastic behavior. A typical connection response is illustrated in Fig. 2.

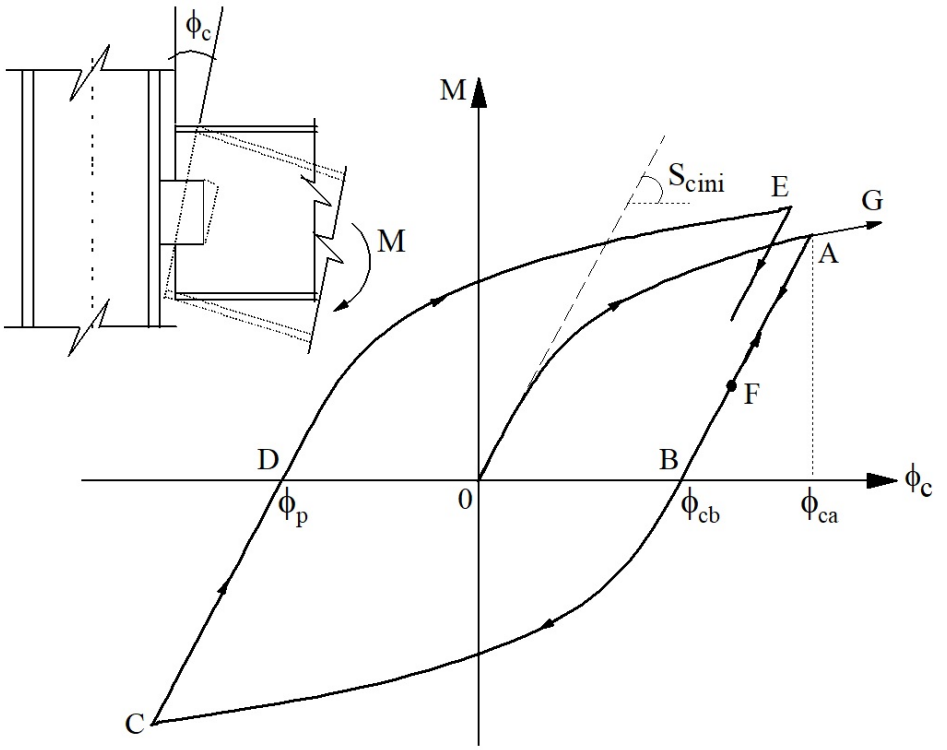

Figure 2: *Connection behavior under cyclic loading.*

In Figure 2 the *0A* curve describes the connection's behavior during the initial loading process of the structure, which is compatible with the different types of connection shown in Fig. 1. The following *AB* and *BC* paths correspond to the unloading process characterized by a decreasing intensity of the bending moment that acts on the connection and the reversal of the direction of the external forcing, as shown by the arrows. The subsequent *CD* and *DE* paths correspond to the next unloading and loading cycles. After the first unloading stage is complete, only a part of the total deformation ϕ_{ca} is recovered and the connection sustains a permanent residual deformation ϕ_{cb}. This also occurs after each of the following loading and unloading cycles. The loops resulting from the non-coincident moment-rotation curves characterize the connection hysteretic behavior, as shown, through cyclic loading tests, by Tsai and Popov (1990), Korol *et al.* (1990) and Abolmaali *et al.* (2003).

The nonlinear behavior of the semi-rigid connections when submitted to cyclic loads can be efficiently simulated by the independent hardening technique, employed previously by, among others, Ackroyd and Gerstle (1982), Azizinamini *et al.* (1987), Chen *et al.* (1996), Chan and Chui (2000) and Sekulovic and Nefovska-Danilovic (2008). An important advantage of this approach is that one can adopt any mathematical function representing the moment-rotation relationship under monotonic loads.

Consider a typical trajectory under increasing load (trajectories indicated by the continuous lines in Fig. 3a) beginning at a point with coordinate ϕ_p, the last permanent residual rotation (at *0A*, the initial loading phase, $\phi_p = 0$), the bending moment M at any position along the trajectory *DE* can be calculated as follows:

$$M = f(\phi_c - \phi_p) \tag{6}$$

where *f* is defined in accordance with a mathematical model that describes the nonlinear moment-rotation behavior of the connection when submitted to a monotonic load. Thus, the connection stiffness is given by:

$$S_c = \left.\frac{dM}{d\phi_c}\right|_{\phi_c=(\phi_c-\phi_p)} \tag{7}$$

The loading process between a time step t (prior) and $t+\Delta t$ (actual) leads to an increase in the bending moment, ΔM, which has the same sign of the bending moment, M. Therefore, the loading condition is verified if $M \cdot \Delta M > 0$.

In the unloading process, based on experimental results, a linear moment-rotation relation with an inclination equal to the initial stiffness of the connection is considered, as illustrated by the solid lines in Figure 3b. Consider, for example, the segment *AB* of the hysteretic cycle. The straight line starting at point $A(\phi_c; M_a)$ (the end of the preceding loading cycle) with an inclination S_{cini} is defined as:

$$M = M_a - S_{cini}(\phi_{ca} - \phi_c) \tag{8}$$

where M_a is the reverse moment at which unloading starts, which can be obtained from Eq. (6) considering $\phi_c = \phi_{ca}$.

During the unloading process, the relation $M \cdot \Delta M < 0$ is obeyed. In some case, however, additional clarifications are necessary. Consider again Fig. 2. If the connection is being unloaded from *A* to *B* and the loading process begins before the unloading has been completed, say at F, the moment-rotation behavior of this element will follow the *FA* trajectory until it reaches the last reverse moment encountered. At this point, the loading process follows the original moment-rotation curve obtained, considering the last permanent rotation ϕ_p.

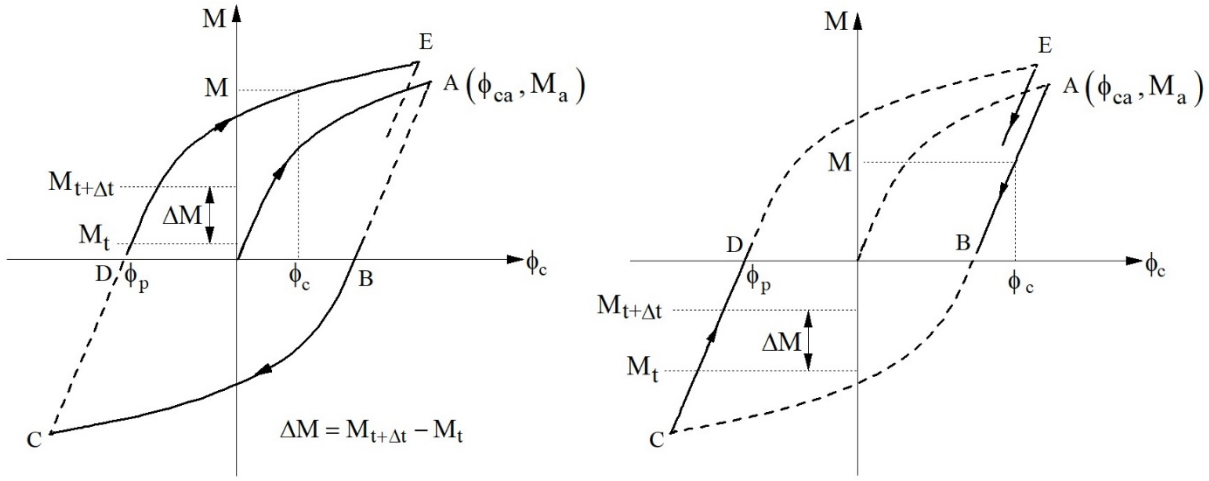

(a) Loading (b) Unloading

Figure 3: *Independent hardening model: loading and unloading portions.*

In computing the independent hardening model, the rotation ϕ_p should be stored after each complete unloading cycle. The reverse moment, M_a, should also be stored every time ΔM changes sign. In addition, the intervals between the two successive time instants should be small so that these variables can be defined with adequate precision.

3 METHODOLOGY FOR NONLINEAR DYNAMIC ANALYSIS

The equations of motion that governs the dynamic response of a structural system can be obtained using the virtual work principle or the virtual displacement principle. Considering the internal, inertial and dissipative forces, the equilibrium at time $t+\Delta t$, can be expressed as (Zienkiewicz and Taylor, 1991):

$$\int_{{}^tV} \tau_{ij}\delta\varepsilon_{ij}dV + \int_{{}^tV} \rho\ddot{d}_k\delta\ddot{d}_k dV + \int_{{}^tV} \mu\dot{d}_k\delta\dot{d}_k dV = \delta d_k{}^T f_{ek} \tag{9}$$

where τ_{ij} represents the Cauchy tensor in equilibrium with external excitation f_{ek}; ε_{ij} represents the virtual Green-Lagrange deformation components corresponding to arbitrary displacements δd_k, which are cinematically compatible with the boundary conditions; ρ is the mass density of the material and μ is the viscous damping coefficient. To determine the equilibrium configuration of the structure at $t + \Delta t$, the updated Lagrangian referential is used. In this case, the configuration at instant t is used as the reference for analysis.

The advantage of using the updated Lagrangian referential depends on the finite element formulation adopted (Bathe, 1996). Wong and Tin-Loi (1990) and Alves (1993) showed that the results obtained using the initial Lagrangian referential leads to accumulated errors if linear interpolation functions (Silveira, 1995) are adopted in the FE formulation due to possible rigid body motions during the incremental process. With an updated Lagrangian referential, these simplified interpolation functions can be applied, as the referential is updated at every increment and rigid body rotations are divided into smaller parts.

According to the usual finite element procedures, and using Eq. (9), the following matrix equation in terms of the nodal displacements is obtained:

$$\mathbf{M}\ddot{\mathbf{U}} + \mathbf{C}\dot{\mathbf{U}} + \mathbf{F}_i(\mathbf{U}) = \lambda(t)\mathbf{F}_r \tag{10}$$

where $\mathbf{M}$ and $\mathbf{C}$ are the mass and damping matrices, respectively; $\mathbf{F}_i$ is the internal force vector; $\mathbf{U}$, $\dot{\mathbf{U}}$ and $\ddot{\mathbf{U}}$, represent the displacement, velocity and acceleration vectors, of the structural system, respectively; $\mathbf{F}_r$ is the vector that defines the external excitation; and λ is the load intensity at a instant *t*.

The stiffness matrix is a function of three variables—the nodal displacements, the internal forces of each element, and connection stiffness and must be continuously updated using an incremental-iterative solver strategy to capture the second-order effects ($P-\Delta$ and $P-\delta$) and connection behavior. To this end, a numerical procedure that combines the Newmark (Chopra, 1995) and Newton-Raphson (Burden and Faires, 2004) methods is adopted. The necessary computational steps are detailed in Appendix A. Notice that the connection stiffness is updated at the end of each iterative cycle. Appendix B summarizes, in algorithmic form, the connection hysteretic model implemented here and described in Section 2.

4 THE SEMI-RIGID FINITE ELEMENT

In most structural analysis programs springs are used to model the connections. Figure 4 shows the planar beam-column element, with nodal points *i* and *j*, and two springs fixed at the extremities. They permit the connections' degree of freedom to be incorporated into the tangent stiffness of the beam-column element. Only the connection's rotational deformation due to bending is considered.

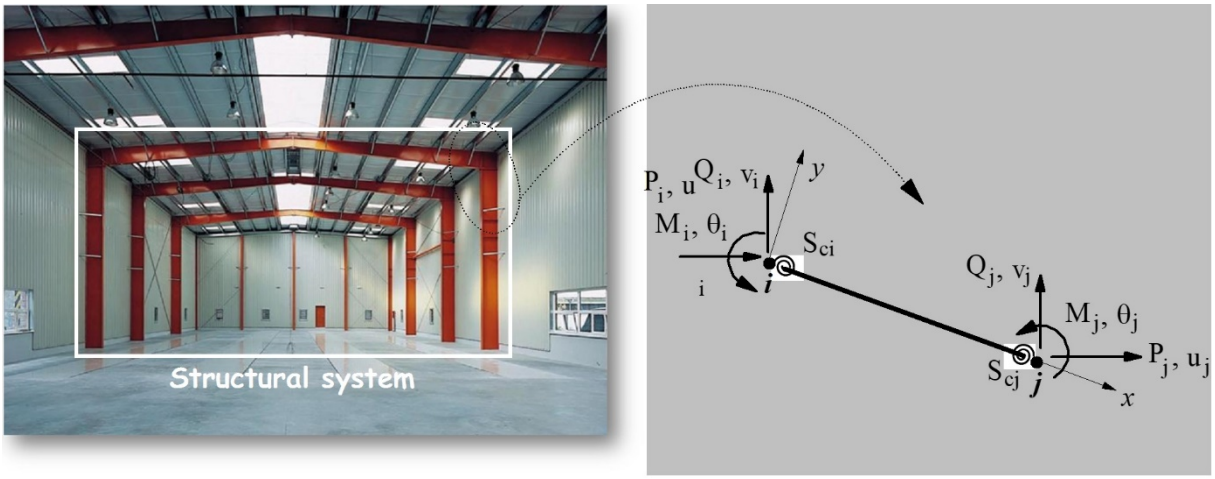

Figure 4: *Beam-column element with semi-rigid connections.*

Figure 5 shows a deformed configuration of the finite element, the internal forces and deformations in the springs, where S_{ci} and S_{cj} denote the stiffness of the spring elements. The connections can be characterized by different moment-rotation curves (Eq. 6). The connection's relative rotation, ϕ_c, is defined as the difference be-

tween the rotational angles of the side connected with the global node of the element, θ_c, and the one connected to the beam-column element, θ_b. Using Eq. (6) and the moment equilibrium of the spring elements, the following relations are obtained:

$$\begin{Bmatrix} \Delta M_{ci} \\ \Delta M_{bi} \end{Bmatrix} = \begin{bmatrix} S_{ci} & -S_{ci} \\ -S_{ci} & S_{ci} \end{bmatrix} = \begin{Bmatrix} \Delta\theta_{ci} \\ \Delta\theta_{bi} \end{Bmatrix} \tag{11}$$

$$\begin{Bmatrix} \Delta M_{cj} \\ \Delta M_{bj} \end{Bmatrix} = \begin{bmatrix} S_{cj} & -S_{cj} \\ -S_{cj} & S_{cj} \end{bmatrix} = \begin{Bmatrix} \Delta\theta_{cj} \\ \Delta\theta_{bj} \end{Bmatrix} \tag{12}$$

where M_c and M_b are the bending moments acting on the spring elements and on the beam-column element, respectively, and the subscripts *i* and *j* refer to the element's extremities.

The effect induced by connection flexibility is accounted for by modifying the element stiffness matrix. Herein, the spring elements simulating the connection's flexibility have null lengths and the moment-rotation equilibrium relation is given by:

$$\begin{Bmatrix} \Delta M_{bi} \\ \Delta M_{bj} \end{Bmatrix} = \begin{bmatrix} k_{(3,3)} & k_{(3,6)} \\ k_{(3,3)} & k_{(3,3)} \end{bmatrix} \begin{Bmatrix} \Delta\theta_{bi} \\ \Delta\theta_{bj} \end{Bmatrix} = \begin{bmatrix} \dfrac{4EI}{L} - \dfrac{2PL}{15} + \dfrac{4PL}{AL} & \dfrac{2EI}{L} - \dfrac{PL}{30} + \dfrac{2PI}{AL} \\ \dfrac{2EI}{L} - \dfrac{PL}{30} + \dfrac{2PI}{AL} & \dfrac{4EI}{L} - \dfrac{2PL}{15} + \dfrac{4PL}{AL} \end{bmatrix} \begin{Bmatrix} \Delta\theta_{bi} \\ \Delta\theta_{bj} \end{Bmatrix} \tag{13}$$

where *E* is the Young's modulus; *I* and *A* are, respectively, the element cross section inertia and area; *L* is the element's length; and *P* is the axial force. The terms of the matrix are the coefficients of a conventional beam-column element stiffness matrix with perfectly rigid connections, determined using the nonlinear geometrical formulation proposed by Yang and Kuo (1994), assuming large displacements and rotations, but small deformations.

Combining Eqs. (11)-(13), results in:

$$\begin{Bmatrix} \Delta M_{ci} \\ \Delta M_{bi} \\ \Delta M_{bj} \\ \Delta M_{cj} \end{Bmatrix} = \begin{bmatrix} S_{ci} & -S_{ci} & 0 & 0 \\ -S_{ci} & S_{ci} + k_{(3,3)} & k_{(3,6)} & 0 \\ 0 & k_{(6,3)} & S_{cj} + k_{(6,6)} & -S_{cj} \\ 0 & 0 & -S_{cj} & S_{cj} \end{bmatrix} = \begin{Bmatrix} \Delta\theta_{ci} \\ \Delta\theta_{bi} \\ \Delta\theta_{bj} \\ \Delta\theta_{cj} \end{Bmatrix} \tag{14}$$

Assuming that the loads are only applied at the global nodes of the element (see Fig. 5), the internal moments M_{bi} and M_{bj} are equal to zero, and the following moment-rotation equilibrium relations is obtained:

$$\begin{Bmatrix} \Delta M_{ci} \\ \Delta M_{cj} \end{Bmatrix} = \left(\begin{bmatrix} S_{ci} & 0 \\ 0 & S_{cj} \end{bmatrix} - \frac{1}{\beta} \begin{bmatrix} S_{ci} & 0 \\ 0 & S_{cj} \end{bmatrix} \begin{bmatrix} S_{cj} + k_{(6,6)} & k_{(3,6)} \\ -k_{(6,3)} & S_{ci} + k_{(3,3)} \end{bmatrix} \begin{bmatrix} S_{ci} & 0 \\ 0 & S_{cj} \end{bmatrix} \right) \begin{Bmatrix} \Delta\theta_{ci} \\ \Delta\theta_{cj} \end{Bmatrix} \tag{15}$$

in which $\beta = \left(S_{ci} + k_{(3,3)}\right)\left(S_{cj} + k_{(6,6)}\right) - k_{(6,3)}k_{(3,6)}$.

Figures 4 and 5 show that $M_i = M_{ci}$ and $M_j = M_{cj}$. Thus, the relationship between the shearing forces and the bending moments, obtained by the equilibrium force and moment, can be written in an incremental matrix form as follows:

$$\begin{Bmatrix} \Delta Q_i \\ \Delta M_i \\ \Delta Q_j \\ \Delta M_j \end{Bmatrix} = \begin{bmatrix} 1/L & 1/L \\ 1 & 0 \\ -1/L & -1/L \\ 0 & 1 \end{bmatrix} = \begin{Bmatrix} \Delta M_{ci} \\ \Delta M_{cj} \end{Bmatrix} \tag{16}$$

with ΔM_i and ΔM_j being the incremental nodal moments, ΔQ_i and ΔQ_j being the incremental shearing forces in the equilibrium configuration *t*.

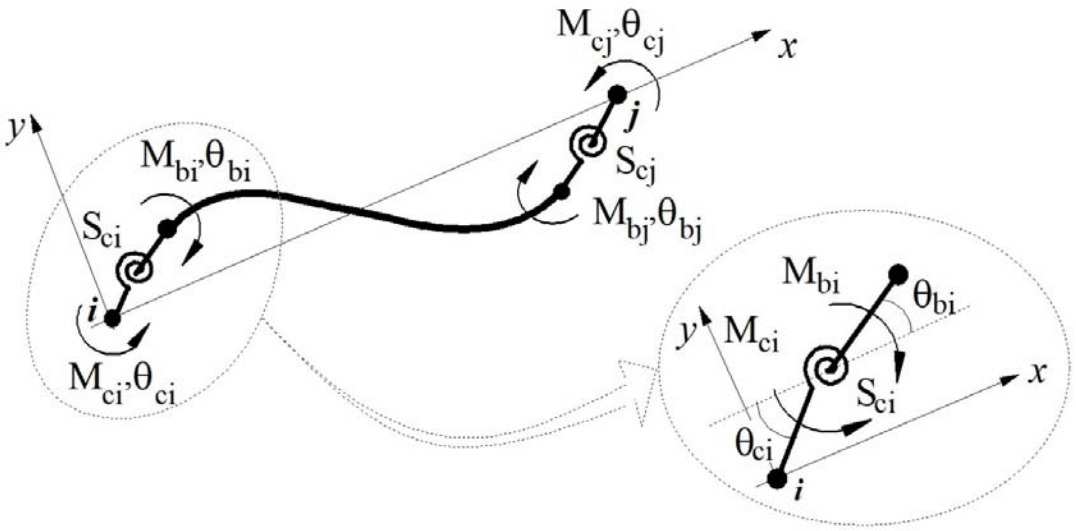

Figure 5: *Deformed configuration and spring element degree of freedom.*

Observing Fig. 6, it is possible to establish the relations:

$$\begin{Bmatrix} \Delta\theta_{ci} \\ \Delta\theta_{cj} \end{Bmatrix} = \begin{bmatrix} 1/L & 1 & -1/L & 0 \\ 1/L & 0 & -1/L & 1 \end{bmatrix} \begin{Bmatrix} \Delta v_i \\ \Delta\theta_i \\ \Delta v_j \\ \Delta\theta_j \end{Bmatrix} \tag{17}$$

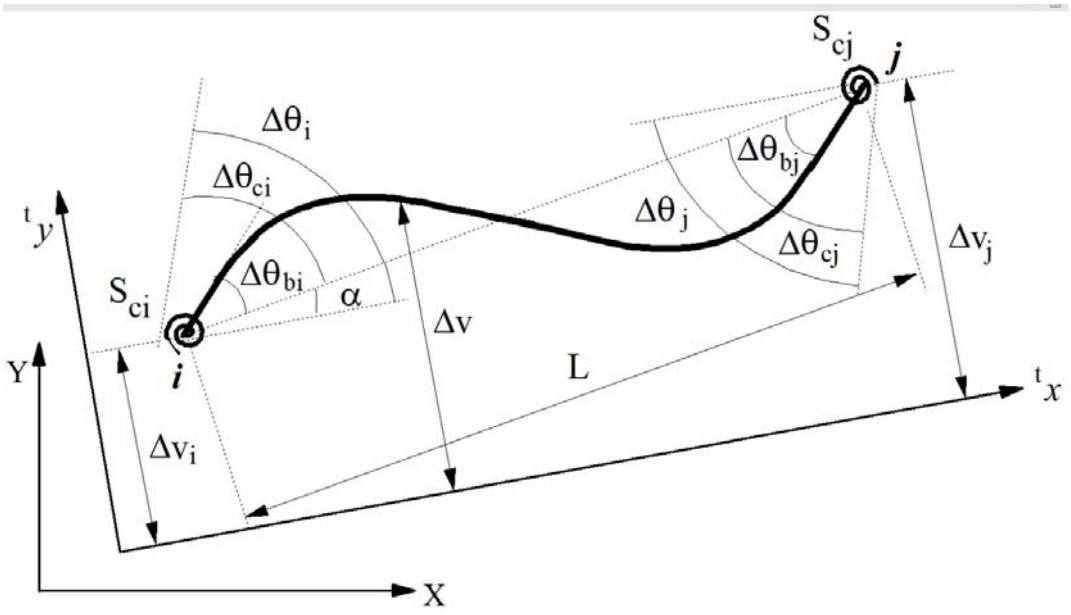

Figure 6: *Nodal displacements of the semi-rigid beam-column element.*

By substituting (15) into (16), using (17), and performing all the necessary operations, the semi-rigid element stiffness matrix is then obtained considering both the connection flexibility and the geometric nonlinear effects. Using these new terms in the complete 6x6 order matrix of the conventional beam-column element, the element stiffness matrix is finally obtained in the local coordinates system. In this formulation, the relation between the axial forces P_i and P_j, and the nodal displacements suffer no alterations when considering the connection flexibility effects. The transformation of the internal force vector and the stiffness matrix to the global coordinates system is carried out following the usual procedures.

4.1 Semi-Rigid Finite Element Mass Matrix

The consistent mass matrix for the beam-column element is defined as (Kishi and Chen, 1986):

$$\mathbf{M}_e = \int_{tV} \mathbf{H}^T \rho \mathbf{H} dV \tag{18}$$

where **H** is the interpolation functions matrix.

According to Chan and Chui (2000), the transversal displacement v of the beam element can be written, in an incremental form, using the following matrix expression:

$$\Delta v(x) = \left[H_1^2 H_2 L - H_2^2 H_1 L \right] \begin{Bmatrix} \Delta\theta_{bi} \\ \Delta\theta_{bj} \end{Bmatrix} + \left[\left(3 - 2H_1\right) H_1 \left(3 - 2H_2\right) H_2 \right] \begin{Bmatrix} \Delta v_i \\ \Delta v_j \end{Bmatrix} \tag{19}$$

where Δv_i and Δv_j are the incremental vertical displacements of the nodes *i* and *j*, and $\Delta\theta_{bi}$ and $\Delta\theta_{bj}$ are the rotations of these same nodes, as shown in Fig. 6. In addition, $H_1 = 1 - x / L$ and $H_2 = x / L$.

To introduce the connection's flexibility effect into the previous expression and thereby obtain the desired mass matrix, the beam-column nodal rotations are related to the rotations at the ends of the element with semi-rigid connections as:

$$\begin{Bmatrix} \Delta\theta_{bi} \\ \Delta\theta_{bj} \end{Bmatrix} = \begin{bmatrix} S_{ci} + \dfrac{4EI}{L} & \dfrac{2EI}{L} \\ \dfrac{2EI}{L} & S_{cj} + \dfrac{4EI}{L} \end{bmatrix}^{-1} \begin{bmatrix} S_{ci} & 0 \\ 0 & S_{cj} \end{bmatrix} \begin{Bmatrix} \Delta\theta_{ci} \\ \Delta\theta_{cj} \end{Bmatrix} \tag{20}$$

Substituting Eq. (17) into Eq. (20) and using Eq. (19), the function that describes the transversal displacement field of a beam with semi-rigid connections is obtained, i.e.:

$$\Delta v(x) = \mathbf{H}^* \left\{ \Delta v_i \;\; \Delta\theta_i \;\; \Delta v_j \;\; \Delta\theta_j \right\}^T \tag{21}$$

in which,

$$\Delta v(x) = \left[H_1^2 H_2 L - H_2^2 H_1 L \right] \begin{bmatrix} S_{ci} + \dfrac{4EI}{L} & \dfrac{2EI}{L} \\ \dfrac{2EI}{L} & S_{cj} + \dfrac{4EI}{L} \end{bmatrix}^{-1} \begin{bmatrix} S_{ci} & 0 \\ 0 & S_{cj} \end{bmatrix} \begin{bmatrix} 1/L & 1 & -1/L & 0 \\ 1/L & 0 & -1/L & 1 \end{bmatrix} + \tag{22}$$

$$\left[\left(3 - 2H_1\right) H_1 \;\; 0 \;\; \left(3 - 2H_2\right) H_2 \;\; 0 \right]$$

The mass matrix components influenced by the connection's stiffness are obtained using the **H*** matrix, instead of the **H** in Eq. (18). The other terms are identical to those developed for the conventional beam-column element with rigid connections (Silva, 2009).

5 NUMERICAL APPLICATIONS

In this section, we use the proposed methodology to obtain the nonlinear dynamic response of four planar structural steel systems: a L-frame, a two-story frame, a six-story frame, and a four-bay five-story frame. In these examples, viscous damping is not considered when the dissipative effect of the connection nonlinear hysteretic behavior on the dynamic response is evaluated.

5.1 L-Frame

The first problem to be analyzed is the L-shaped frame with built-in extremities illustrated in Fig. 7, where the relevant data is also presented. The connection between these two members is either perfectly rigid or semi-rigid. In the semi-rigid case, an end plate connections with an initial stiffness S_{cini} = 137.3 Nm/rad is considered. Kawashima and Fujimoto (1984) experimentally measured the frame's natural frequencies considering a rigid beam-column connection. They also numerically determined these frequencies considering a semi-rigid connec-

tion. In addition to these authors, Shi and Atluri (1989) and Chan and Chui (2000) used this structure to test their numerical formulations for dynamic analyses of plane frames applying an impact load (19.6 N) in the middle of the frame column. The application of a load with low value is justified by the low resistance of the semi-rigid connection of the beam-column elements. Table 1 compares the present results with the natural frequencies corresponding to the first two vibration modes obtained by the aforementioned authors. The results agree well with those found in literature.

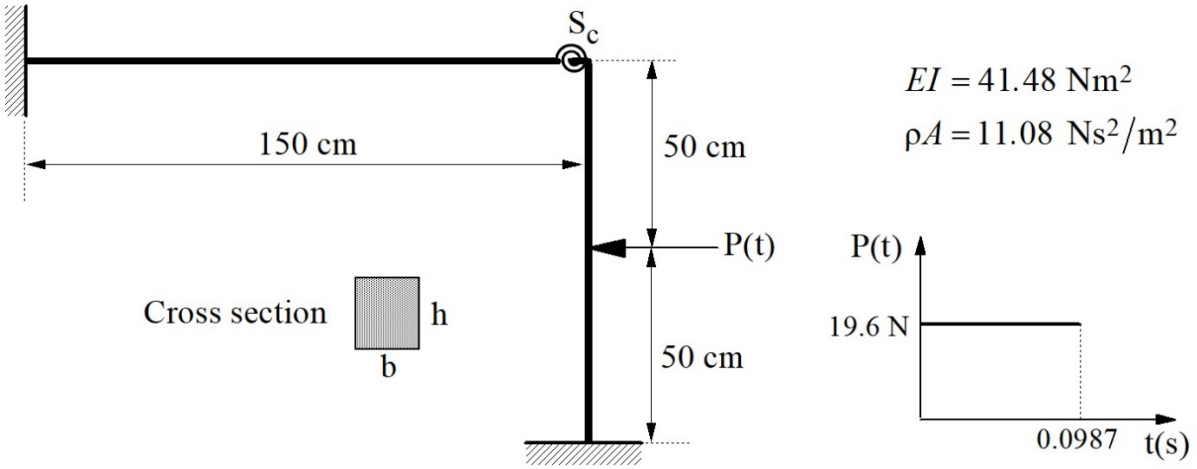

Figure 7: *L-shaped frame: geometry and loading.*

To evaluate the influence of the connection's nonlinear behavior on the dynamic response, a short-duration impact load *P(t)* with a constant intensity of 19.6 N is applied at the center of the column, as shown in Fig. 7. To verify the importance of the adopted semi-rigid connection's moment-rotation function in this representation, two models are considered: the exponential [59] and the four-parameter model (Chen and Lui, 1991). The parameters for the exponential model, described by Eq. (4), are as follows: m=6, $C_1 = 1.078915$, $C_2 = 18.148410$, $C_3 = 52.890917$, $C_4 = -34.035435$, $C_5 = -37.194613$, $C6 = 43.896458$, $\alpha = 0.000384$, $R_p = 95.55031$ kgfcm/rad and $M_o = 0$. For the four-parameter model (Eq. 5), in addition to the previous initial stiffness, the following values are used: $R_p = 8.826$ Nm/rad, $M_o = 0.883$ Nm and $n = 1.7$.

Table 1: *The two lowest natural frequencies of the L-frame (rad/s).*

Types of Connections	Present work	Kawashima and Fujimoto (1984)		Shi and Atluri (1989)	Chan and Chui (2000)
		Numerical	Experimental		
Rigid	$\omega_1 = 15.81$	$\omega_1 = 16.30$	$\omega_1 = 15.50$	$\omega_1 = 15.87$	–
	$\omega_2 = 34.74$	$\omega_2 = 35.90$	$\omega_2 = 30.80$	$\omega_2 = 35.30$	–
Semi-rigid	$\omega_1 = 14.90$	$\omega_1 = 14.90$	–	$\omega_1 = 14.75$	$\omega_1 = 15.22$
	$\omega_2 = 32.77$	$\omega_2 = 33.00$	–	$\omega_2 = 32.06$	$\omega_2 = 33.52$

In the numerical analysis a constant time increment $\Delta t = 10^{-4}$ s is used. Figure 8a shows the initial time response of the horizontal displacement u at the load application point considering a liner connection behavior (the connection stiffness S_c is constant) and compare the results with those obtained by Chan and Chui (2000) and Shi and Atluri (1989). The results obtained by using the connection exponential model are compared in Fig. 8b with those by Chan and Chui (2000) and Shi and Atluri (1989), who adopted the Ramberg-Osgood model to describe the connection's nonlinear behavior. Comparing Figs. 8a and 8b, it is possible to verify the difference in responses when considering the semi-rigid connection with linear and nonlinear model. See that the frame response with the nonlinear connection model has the displacement amplitudes reduced due to the hysteretic damping provided by the joint nonlinear behavior.

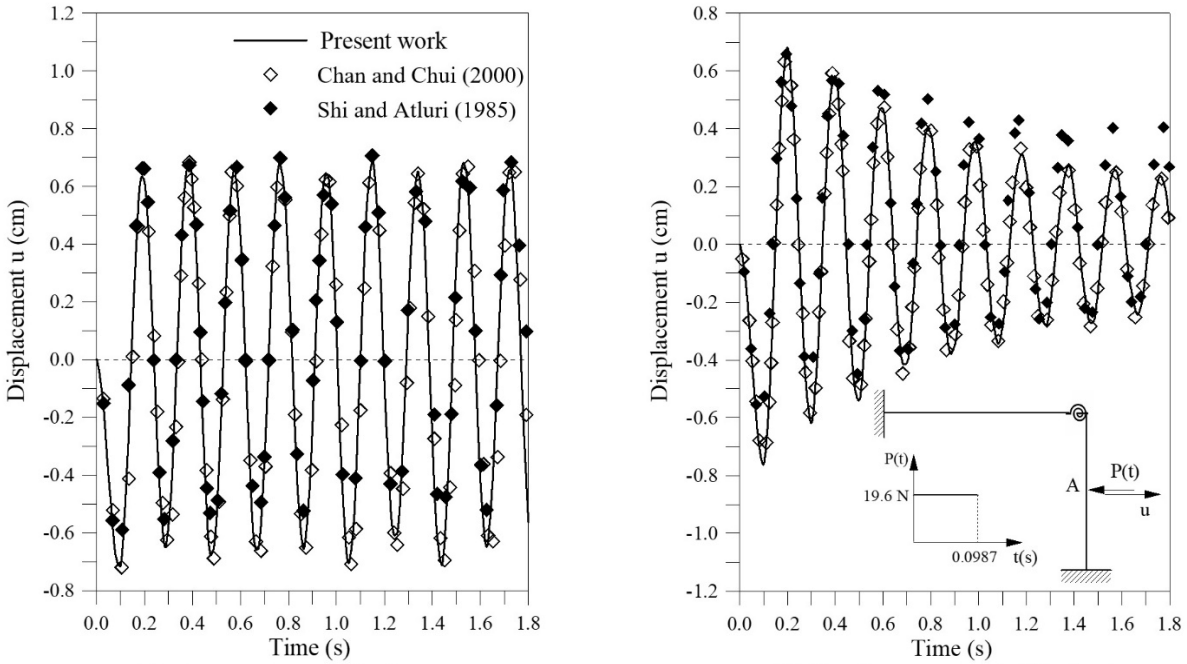

(a) Linear semi-rigid behavior (b) Nonlinear semi-rigid behavior

Figure 8: *L-shaped frame: geometry and loading.*

The comparison between the connection's linear and nonlinear responses is shown in Fig. 9. The vibration period is practically the same in both cases, since the same initial stiffness of the connection is considered. However, the nonlinearity of the connection leads to a strong decrease in the vibration amplitude, due to energy dissipation during each hysteretic cycle, as illustrated in Fig. 9b, where the connection's moment-rotation response is displayed.

To investigate the influence of the chosen mathematical model for the connection's moment-rotation behavior, the same analysis is carried out, now using the four-parameter model. Figure 10 shows, for both the exponential and potential models, the horizontal displacement at the load position and the connection's hysteretic behavior. A small difference occurs in the connection's hysteretic behavior (Fig. 10b) but the time responses are coincident (Fig. 10a). Thus, in the present case, the connection's description has negligible influence on the frame response.

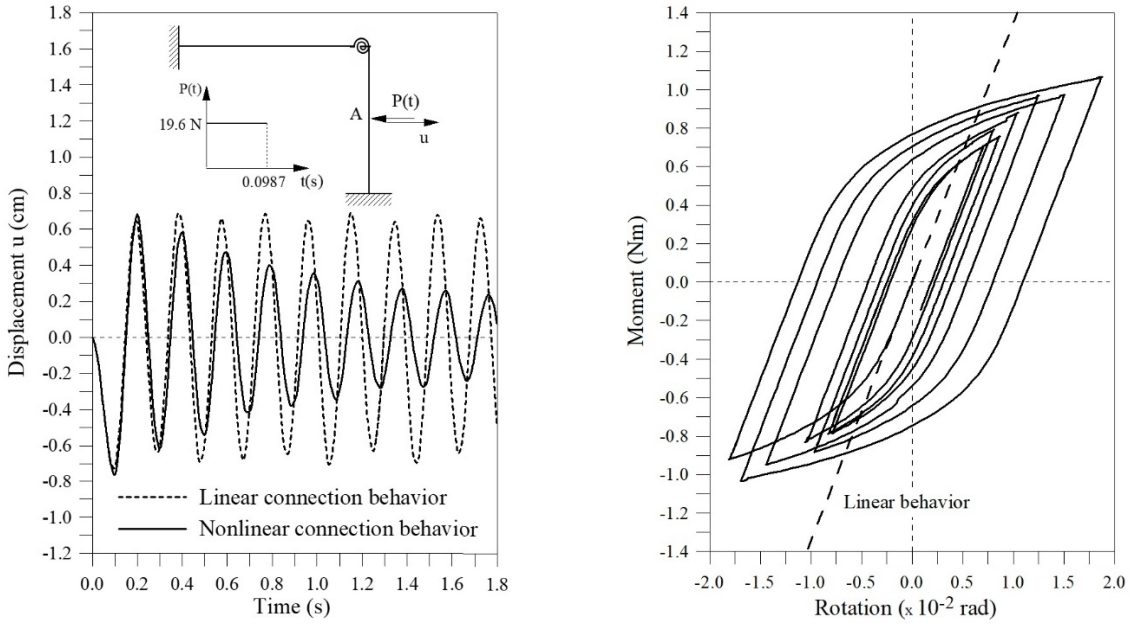

(a) Displacement-time response (b) Connection hysteretic behavior

Figure 9: *Dynamic behavior of the L-frame with semi-rigid connection.*

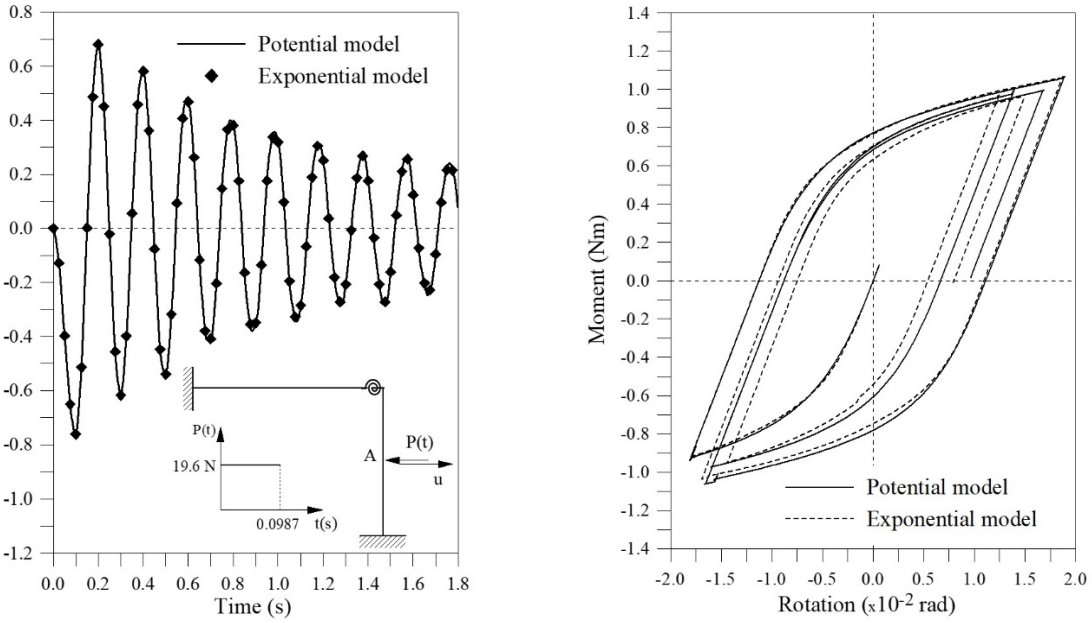

(a) Displacement-time response (b) Connection hystetic behavior

Figure 10: *Different connection models used in the L-frame analysis.*

5.2 Two-Story Frame

The next structure to be investigated is the single-bay, two-story frame subjected to horizontal loads applied at the top of each pavement, as illustrated in Fig. 11. For the beams, a W360x72 profile is adopted, and for the columns, a W310x143 profile. Young's modulus is equal to 205 GPa. Two concentrated masses of 3730 kg are considered at the extremities of each beam and in the middle, a mass of 7460 kg. The structure is then analyzed considering a periodic load and a rectangular pulse, (see Fig. 11).

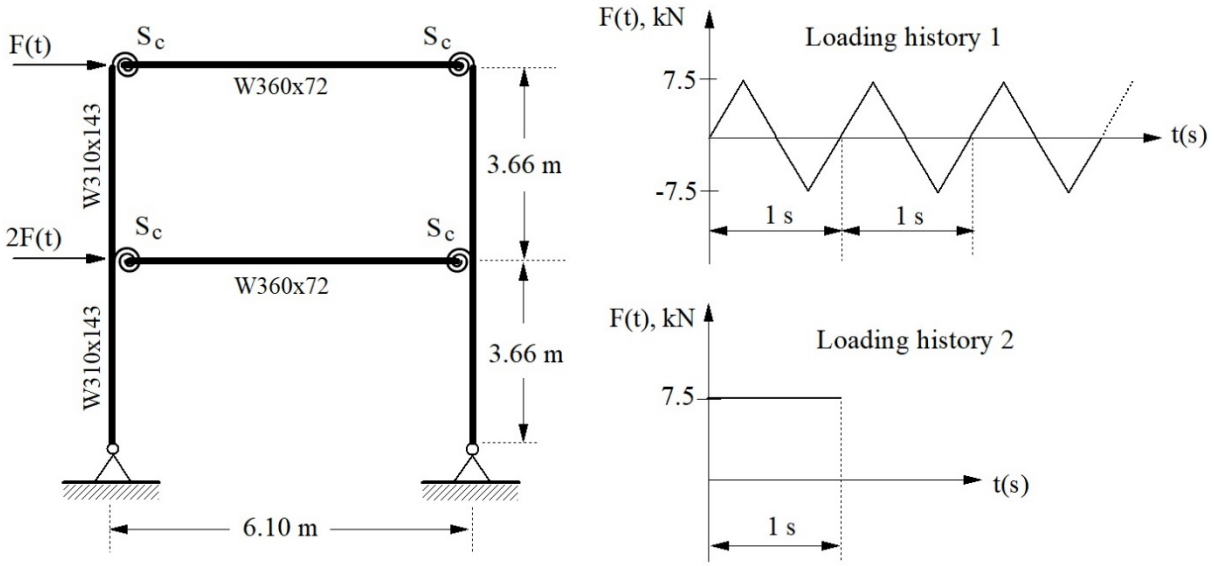

Figure 11: *Single-bay, two-story portal frame: geometry and loads.*

Extended flush end plate connections, with an initial stiffness of 34804 kNm/rad, are considered between the beams and the columns. Its nonlinear moment-rotation behavior is represented by the exponential model, with parameters: m = 6, C_1 = -0.25038x10^{-3}, C_2 = 0.50736x10^{6}, C_3 = -0.30396x10^{5}, C_4 = 0.75338x10^{5}, C_5 = -0.82873x10^{5}, C_6 = 0.33927x10^{5}, α = 0.31783x10^{-3}, R_p = 0.96415x10^{3} kip/rad and M_o = 0.

Figure 12a illustrates the time response obtained for the horizontal displacement at the top of the structure when submitted to a periodic load, where the present results are compared with those by Chan and Chui (2000). In the transient regime the displacement reaches a maximum of around ± 7 cm. After approximately 6s, the structure reaches the permanent regime with an amplitude of ± 5 cm, when the energy introduced into the structure by the external loads and the energy dissipated through the semi-rigid connections are balanced. The connection's moment-rotation behavior during the total response is shown in Fig. 12b.

To investigate the effect of gravitational loads and the P- δ effect on the nonlinear dynamic response, gravitational static loads of 36.6 kN at the extremities and of 73.2 kN in the middle of the beam are considered. These loads induces an increase of the axial forces in the columns and additional bending moments, reducing the stiffness of these members and, consequently, of the structural system. The analysis is performed considering a rectangular pulse of 7.5 kN acting during 1s. Three types of beam-column connections are considered: rigid, linear semi-rigid and nonlinear semi-rigid. Figures 13a-b exhibits the time history of the horizontal displacement at the top of the structure respectively with and without the presence of the gravitational forces. In both cases the semi-rigid connection leads to a strong increase in the displacements and, consequently on the stresses and strains. The maximum displacement for the nonlinear semi-rigid connection is more than three times than that of the frame with rigid connections. This underlines the importance of a detailed dynamic analysis of portal frames with semi-rigid connections and explains the usually large vibration amplitudes of these structures.

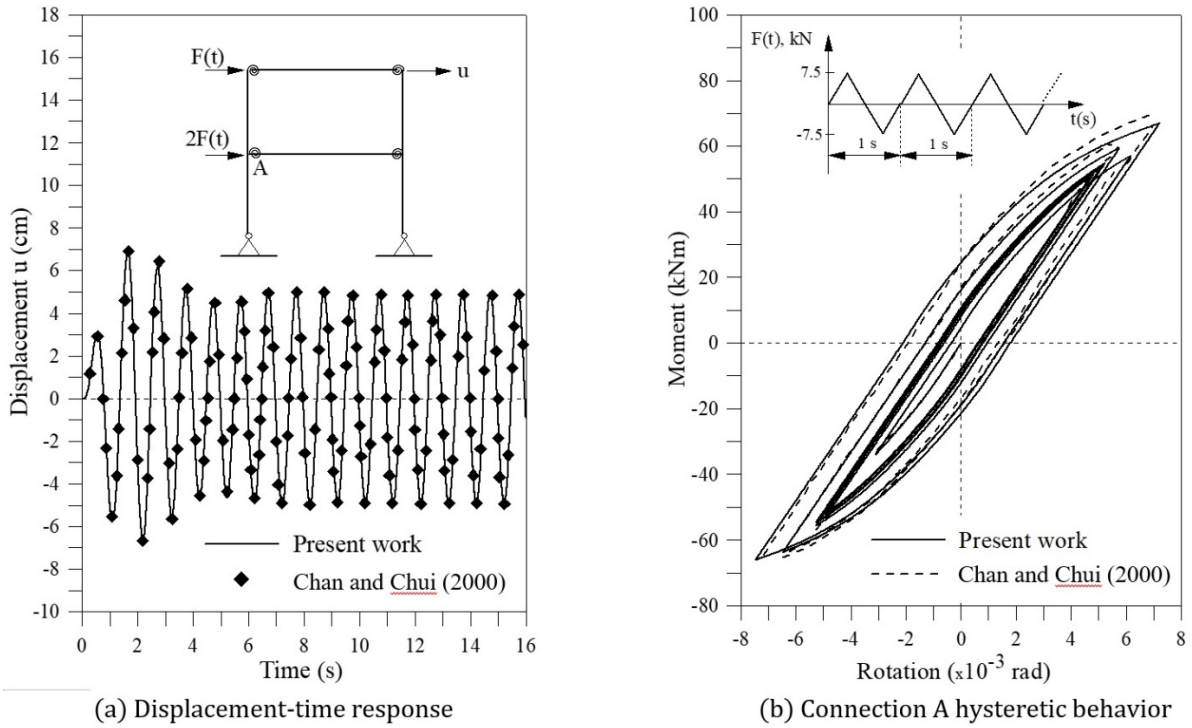

(a) Displacement-time response (b) Connection A hysteretic behavior

Figure 12: *Transient response of the single-bay, two-story portal frame under periodic load.*

For this example, in particular, even considering the influence of the second order effects, the presence of gravitational forces induced a small increase in the displacements. In the rigid connections case, this influence was smaller. While the vibration amplitudes remained constant for the structure with rigid or linear semi-rigid connections, it decreased in the nonlinear semi-rigid case due to the hysteretic damping. If viscous damping was also considered all responses converged to the respective static response.

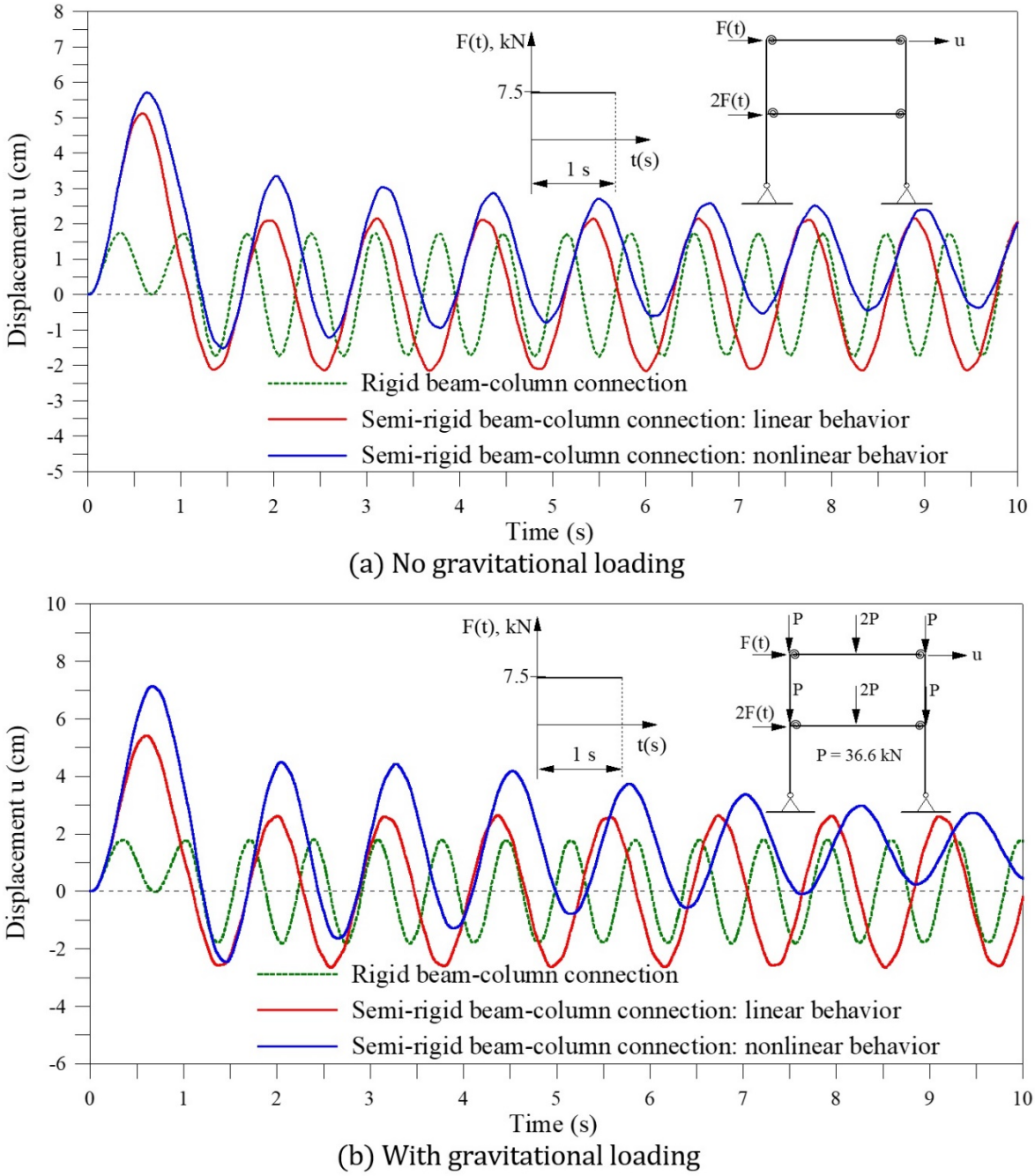

Figure 13: *Transient response of the single-bay, two-story portal frame under a rectangular pulse.*

5.3 The Six-Story Vogel Frame

Now, the influence of beam-column's semi-rigid connections on the dynamic response of a two-bay, six-story steel frame, shown in Fig. 14, is investigated. The analysis of this structure with beam-column rigid connections is a classic problem, proposed by Vogel (1985), to calibrate inelastic formulations. The beams are subjected to uniformly distributed static loads with intensities of 31.7 kN/m (top floor) and 49.1 kN/m (other floors), which are transformed into equivalent nodal loads and added as additional masses to the self-weight of the structural members. At the top of the columns, in each of the six pavements, concentrated lateral harmonic loads are applied having the following intensities: $F_1 = 10.23\ \sin(\omega_{ct})$ kN and $F2 = 20.44\ \sin(\omega_{ct})$kN. The beams and columns'steel profiles are also shown in the figure. Young's modulus is assumed to be equal to 205 GPa and an initial geometric imperfection of $\Delta_0 = 1/450$ for the columns is adopted. Again, three types of beam-column connections are considered: rigid, linear semi-rigid and nonlinear semi-rigid. The same semi-rigid connections used in the previous problem are adopted here (flush end plate).

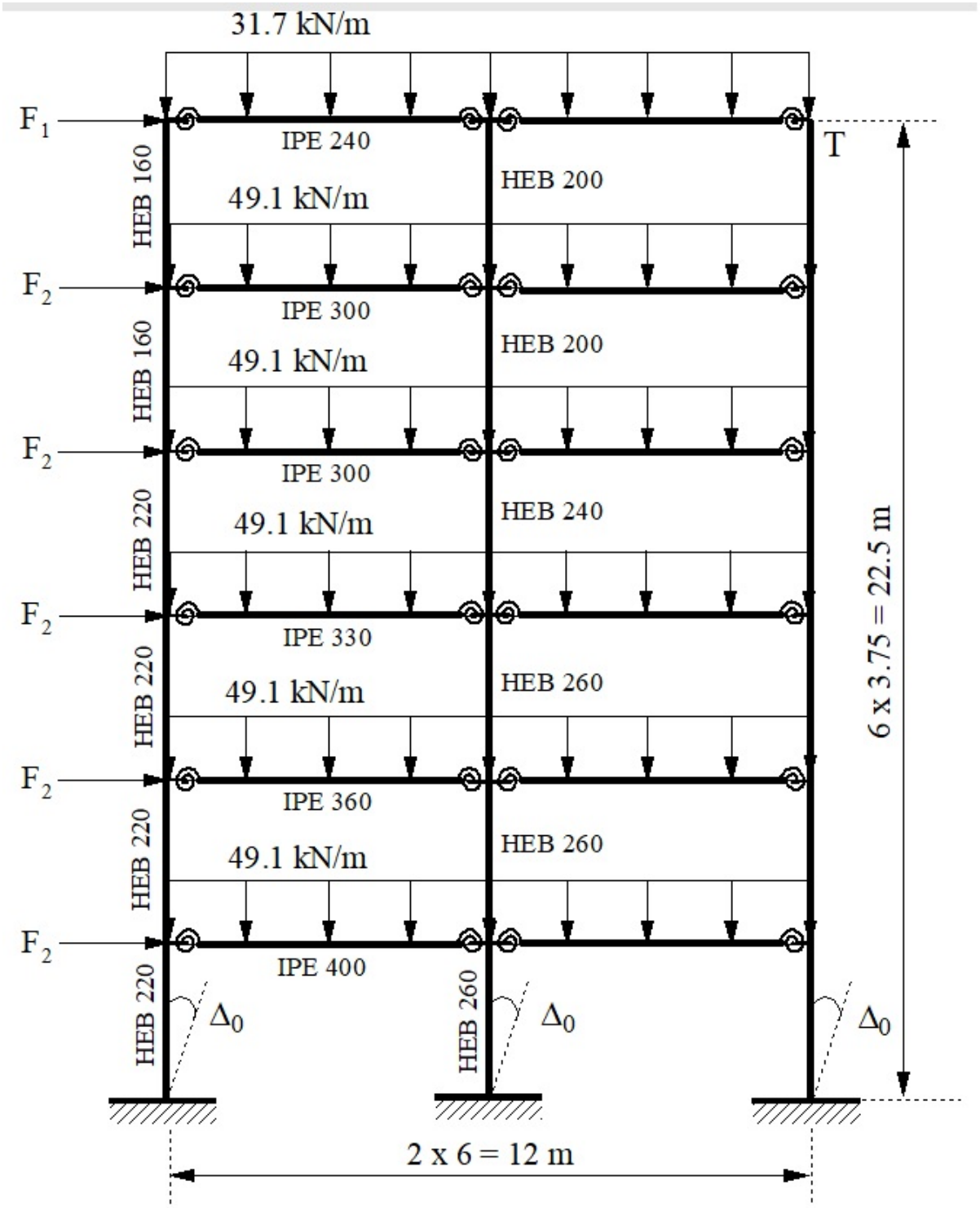

Figure 14: *Two-bay, six-story Vogel frame: geometry and loading.*

The fundamental natural frequency of the frame with rigid connections is 2.41 rad/s; when adopting linear semi-rigid connections, the value reduces to 1.66 rad/s, increasing the effect of lateral loads such as wind loads on the structural response. The frame with nonlinear semi-rigid connections has the same natural frequency, since the initial stiffness is the same as in the linear case. Figs. 15a-d illustrate the transient responses of the structure's top lateral displacement for increasing values of the forcing frequency ω_c. The displacements of the frame with nonlinear beam-column connections can be amplified or dampened, depending on the forcing frequency. For low forcing frequencies, see Fig. 15a (ω_c = 1 rad/s), the horizontal displacement, when considering the nonlinear behavior of the connections (S_c variable), is rather larger than the other two cases. In Fig. 15b the forcing frequency is equal to the natural frequency of the frame with linear semi-rigid connections, ω_c = 1.66 rad/s, and the corresponding vibration amplitudes increases linearly. Therefore, it was expected that the structure with rigid

connections, when submitted to the action of the load whose frequency is equal to the natural frequency, it would show a resonant response (with vibration amplitudes increasing linearly). This was also expected for the frame with semi-rigid connections, however, when the frame is analyzed with semi-rigid connections with non-linear behavior, its amplitude of vibration also increases, but this is limited by the hysteretic damping which, as shown here, has a beneficial effect in the resonance region. For $\omega_c = 2.41$ rad/s, the frame with rigid connections display a resonant response, as illustrated in Fig. 15c. For $\omega_c = 3.33$ rad/s, Fig. 15d, outside the main resonance region, a sharp decrease in the vibration amplitudes are observed in all cases. Shown in Figs. 16a-b are the moment-rotation hysteretic cycles for the beam-column connection identified inset Fig. 16b considering $\omega_c = 1.66$ rad/s and $\omega_c = 2.41$ rad/s, respectively. Comparing the hysteretic cycles, it is observed that the amount of energy dissipated when $\omega_c = 1.66$ rad/s is greater than that for $\omega_c = 2.41$ rad/s, which is in agreement with the time responses in Figs. 15b-c, highlighting the influence of the nonlinear moment-rotation behavior of the semi-rigid connections on the dynamics of steel structures.

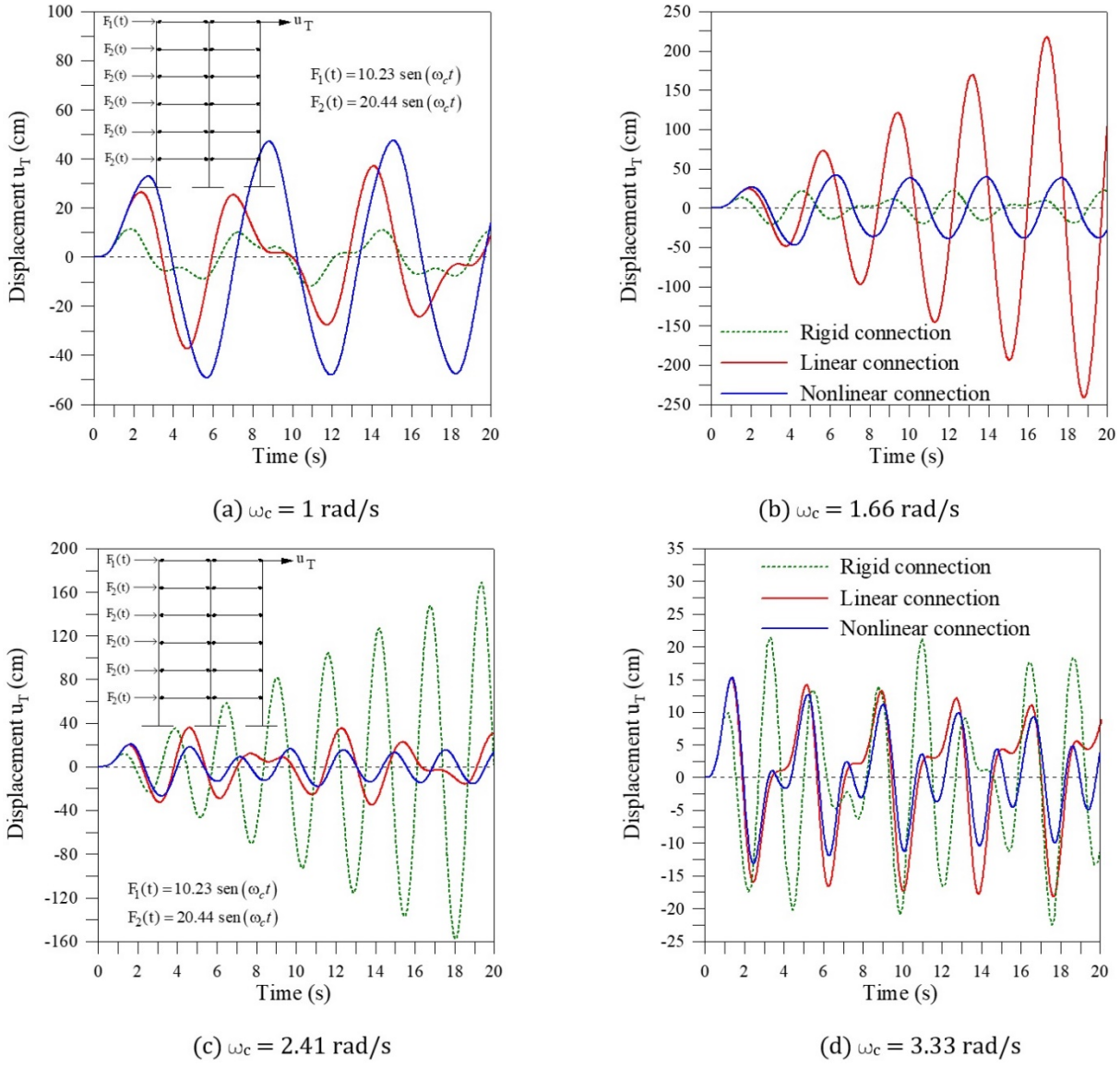

Figure 15: *Transient response of the six story Vogel frame under lateral harmonic forcing.*

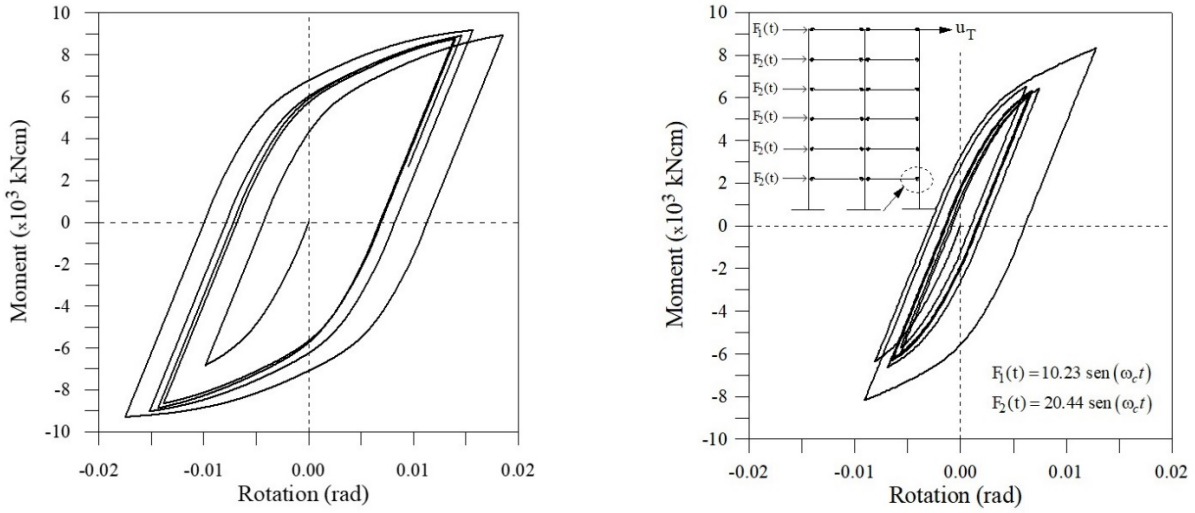

(c) $\omega_c = 1.66$ rad/s (d) $\omega_c = 2.41$rad/s

Figure 16: *Connection hysteretic behavior.*

5.4 Four-Bay Five-Story Frame

This last example investigates a four-bay, five-story steel frame located in Shanghai, China, under seismic excitation. The results show how semi-rigid connections can significantly alter the dynamics of steel structures under base excitation to ensure adequate strength and prevent collapse. Its geometric configuration is shown in Fig. 17a. The flush end plate beam-column connections are adopted and their behavior is represented by the Richard-Abbott model with the parameters: $S_{cini} = 12336{,}86$ kNm/rad, $R_p = 112{,}97$ kNm/rad, $M_0 = 96{,}03$ kNm and $n = 1{,}6$ (Nguyen, 2010). Gravitational loads are also included as additional lumped masses at the beams' nodes. The effect of a mesh refinement in the beams is also considered. The frame is assumed to be subjected to the first ten seconds of the 1940 El Centro N-S earthquake component, shown in Fig. 17b, with a peak ground acceleration of 0.31g.

First, the free vibration analysis on the structure, considering the beam-column rigid connections, is performed. The results are presented in Table 2 for the first two natural periods of vibration. Table 3 presents the results considering semi-rigid connections. In both cases an excellent agreement with the results by Nguyen (2010) is observed. Also, the influence of the beam discretization is negligible. Figure 18 shows the variation of the first five natural frequencies of the frame, parametrized by the respective value considering a rigid connection, as a function of the beam-column connections flexibility, γ. All natural frequency ratios increase with γ and converges to one at $\gamma = 1$. The connection flexibility has a significant influence on the variation of the natural frequencies, particularly on the lowest frequencies. As the natural frequencies decrease increases the influence of environmental loads, whose spectral content is located usually in the low frequencies range. This fact can be very important for frames under seismic loads, as the lower modes may have strong influence on a building's seismic response.

The hysteretic moment-rotation behavior of the semi-rigid joints A and C (see inset in Fig. 19a), are illustrated in Fig. 19a and 19b, respectively for the frame under the El-Centro earthquake. Figure 20 shows the time response of the horizontal displacement at the structure's roof level.

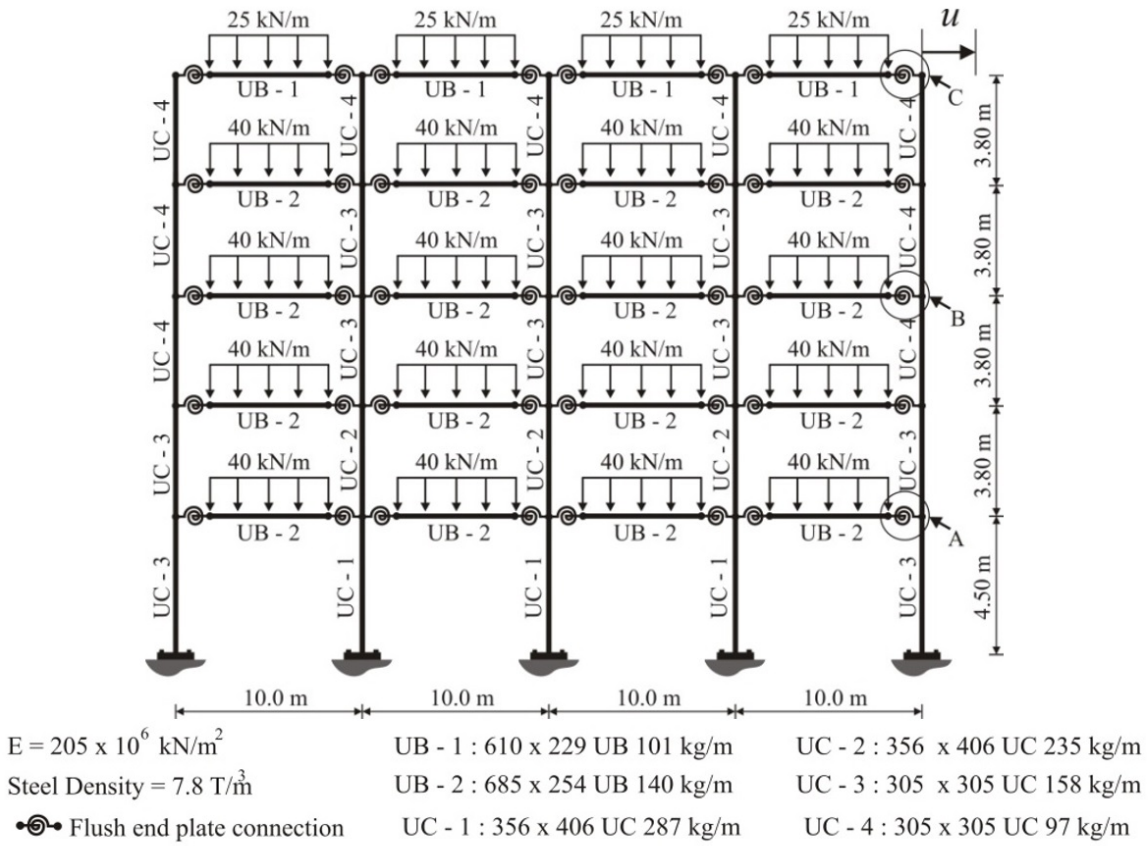

(a) Geometric and material properties

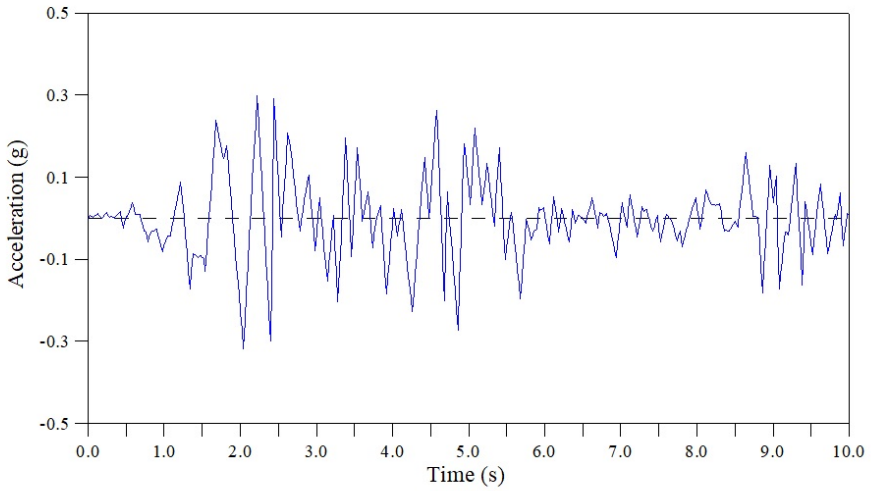

(b) First ten seconds of the N-S El Centro ground motion acceleration (Thai and Kim, 2011)

Figure 17: *Transient response of the single-bay, two-story portal frame under a rectangular pulse.*

Table 2: *First two natural periods of vibration (s) for the frame with rigid connections.*

Modes	Nguyen (2010)	Present Work		
		One element	Two elements	Five elements
1	1.2282	1.1818	1.1820	1.1824
2	0.4196	0.4196	0.4201	0.4201

The first- and second-order elastic transient responses of the building with rigid connections are presented in Fig. 20a and compared with the nonlinear second order response obtained by Nguyen (2010).

Table 3: *First two natural periods of vibration (s) for the frame with flexible connections.*

Modes	Nguyen (2010)	Present Work		
		One element	Two elements	Five elements
1	2.700	2.623	2.623	2.623
2	0.777	0.733	0.773	0.770

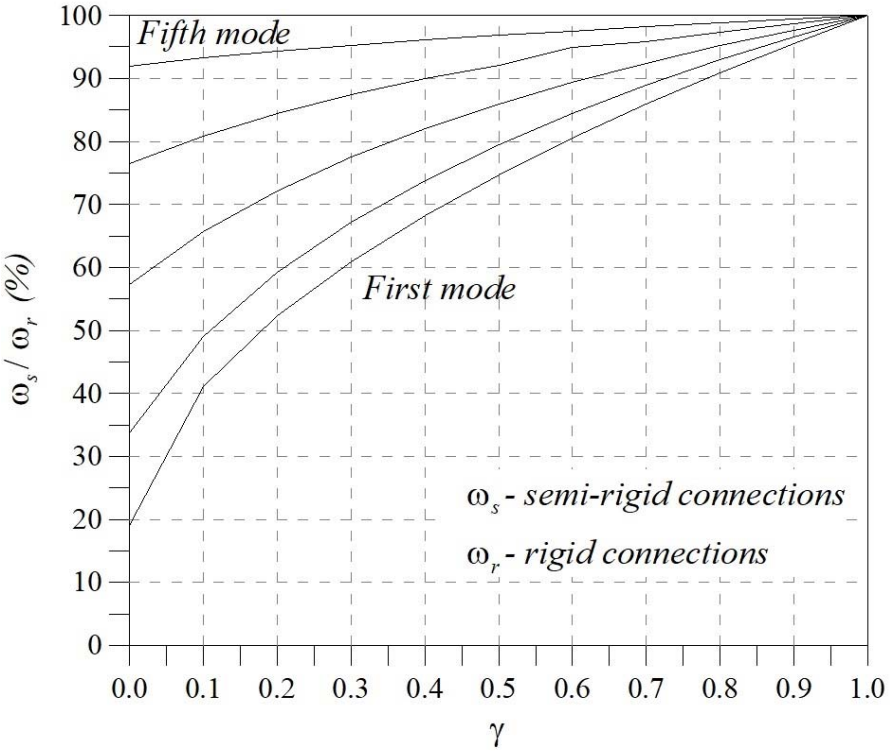

Figure 18: *Influence of beam-column connection flexibility on natural frequencies.*

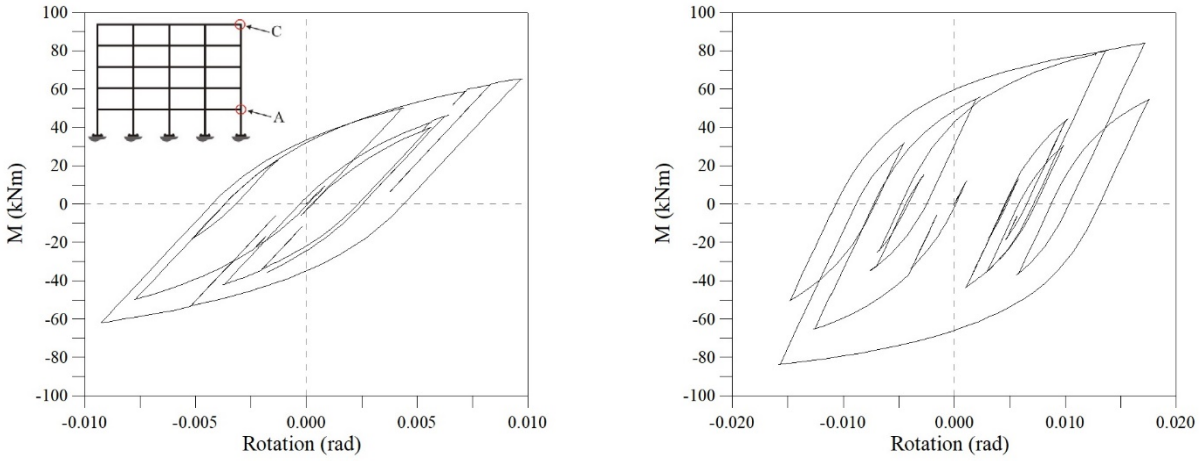

Figure 19: *Beam-column connection hysteretic behavior.*

Figure 20b shows the transient responses for the steel frame with flexible connections, but considering only their linear behavior, in which case it is assumed that $S_c = S_{cini}$= 12336,86 kNm/rad. Finally, Figure 20c presents the transient second-order response of the steel frame with flexible connections, but considering their nonlinear

hysteretic behavior (Richard Abbott model) and an increasing number of finite elements in the beams' discretization process. Again, a good agreement with the results found in (Nguyen, 2010) is observed. Comparing the results, the marked influence of the structure's geometric nonlinearity on the dynamic response is observed. The consideration of the connections' flexibility significantly amplifies the displacements (compare Figure 20a and Figure 20b).

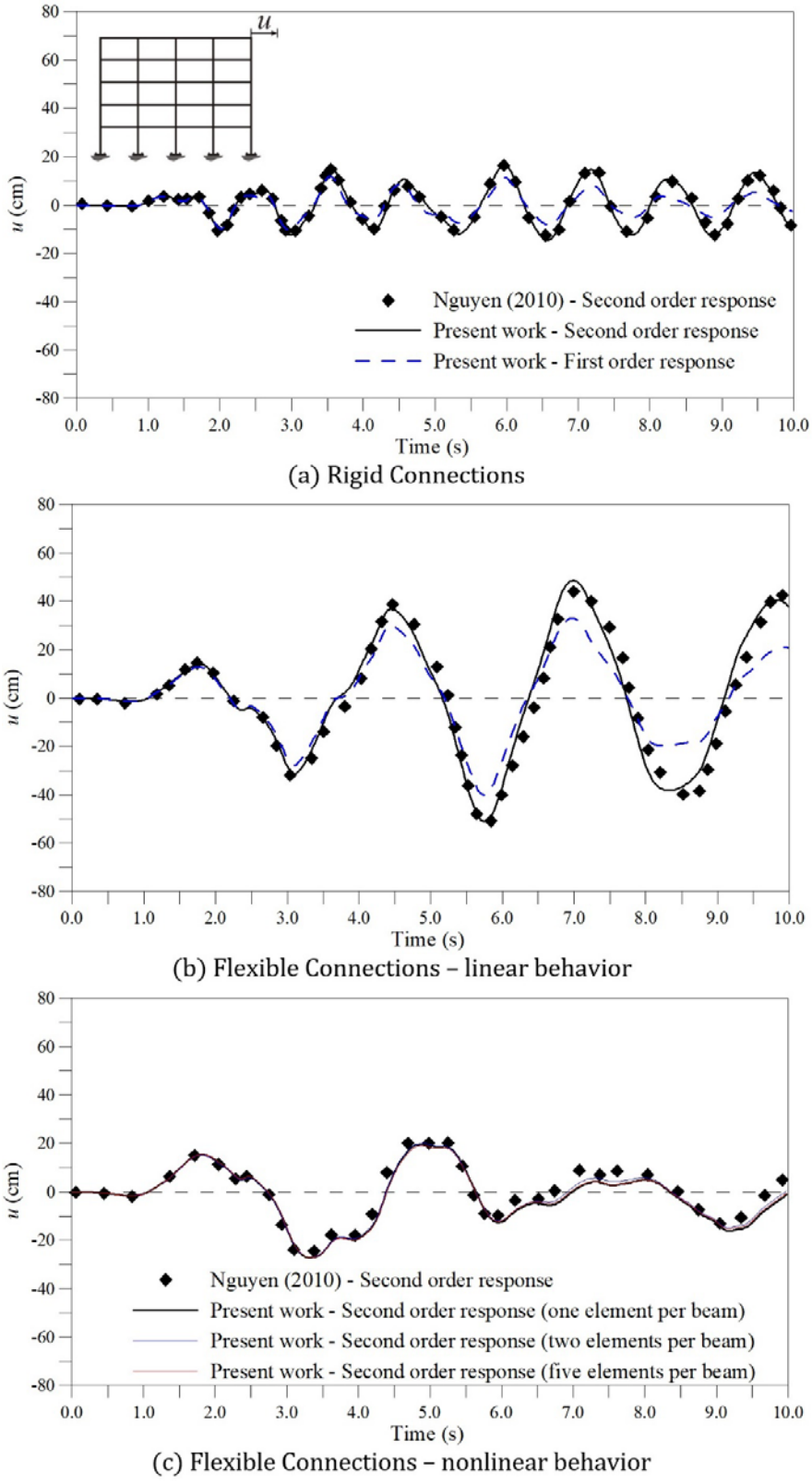

Figure 20: *Time response of the horizontal displacement at the structure's roof level.*

The connections nonlinearity, Figure 20b, decreases the displacements in comparison with the linear case, but the results are higher than those with rigid connections. The second-order effects lead to a slight increase in the vibration amplitudes. Finally, the beams discretization has no detectable effect on the results.

6 FINAL REMARKS

This article presents the fundamentals for prediction of a more realistic behavior of frames with semi-rigid connections under dynamic loading. In the structural behavior evaluation, the effects of geometric nonlinearity and connection flexibility are considered. Different types of connections are considered and compared. Numerical studies are carried out for four structures with different geometries and load conditions. The obtained results are compared with experiments and solutions available in the literature. The coincidence or not with the results of others authors can be strongly influenced by the geometric nonlinear finite element formulation adopted, since the structures studied are slender. But Good agreement is found in all cases, confirming the efficiency of the formulation and numerical solution strategy adopted herein. Thus the numerical approach proposed here can be efficiently used to evaluate the nonlinear transient response of planar steel structures with semi-rigid connections.

The connections flexibility may decrease significantly the natural frequencies, increasing consequently the effect of environmental loads such as wind and earthquakes on the dynamic response of the structure. Thus, these loads may induce resonance and therefore large amplitude oscillations beyond the acceptable maximum values, which dramatically reduce the comfort (sea-sickness) and therefore limit the use of the building, may cause low cycle fatigue or even impair the safety of the structure, producing unacceptable economic losses. For example, the ASCE Standard (ASCE 7-05, 2006) classifies a structure as dynamically sensitive, or "flexible", if the lowest natural frequency < 1 Hz. When considering the hysteretic behavior of the connection, a gradual reduction of the displacement amplitudes is observed. The damping introduced by the connection's nonlinear hysteretic behavior decreases the vibration amplitudes, increasing the safety of the structure. This damping is measured by the connection's capacity to dissipate energy in each cycle, which can be evaluated by calculating the enclosed area of the curve that relates the force acting on the connection to its deformation. Viscous damping was not considered in the present analysis to draw attention to the influence of the connection's dissipative properties. Although beneficial, viscous damping coefficients of slender steel frames are usually very low. The connection behavior is shown to have a strong influence on the results. As the spring model is used to represent the semi-rigid joint behavior, the number of springs depends on the number of structure connections. Thus the consideration of the true connection behavior is extremely important for a realistic forecasting of the dynamic response and resistance of a structural steel frames. Finally, second order effects are shown to increase the vibration amplitudes, reducing the comfort and safety of tall building frames.

Acknowledgments

The authors wish to express their gratitude to CAPES and CNPq, FAPEMIG and UFOP for the support received in the development of this research. Special thanks go to Prof. Harriet Reis and Prof. John White for their editorial reviews.

References

ABNT - NBR 8800. (2008). Project and Execution of Steel Buildings Structures, Brazilian Association of Technical Standards, Rio de Janeiro, Brazil (in Portuguese)

Abolmaali, A., Kukreti, A., Motahari, A., Ghassemieh, M. (2009). Energy dissipation characteristics of semi-rigid connections. Journal of Constructional Steel Research 65: 143-171.

Abolmaali, A., Kukreti, A.R., Razavi, H. (2003). Hysteresis behavior of semi-rigid double web angle steel connections. Journal of Constructional Steel Research 59: 1057-1082.

Ackroyd, M.H. and Gerstle, K.H. (1982). Behavior of type 2 steel frames. Journal of the Structural Engineering 108:1541-1556.

AISC. (2010). Specification for Structural Steel Buildings, American Institute of Steel Construction, ANSI/AISC 360-05, Chicago, IL.

Alves, R. V. (1993). Formulation forgeometric nonlinear analysis in Total Lagrangian reference. 1º Doctoral Seminar (in Portuguese), COPPE/UFRJ, Rio de Janeiro/RJ, Brazil.

Arbabi, F. (1982). Drift of flexibly connected frames. Computers & Structures, 15(2): 102-108.

Aristizabal-Ochoa, J. D. (2015). Stability of imperfect columns with nonlinear connections under eccentric axial loads including shear effects. International Journal of Mechanical Sciences 90: 61 76.

ASCE 7-05. (2006). Minimum Design Loads for Buildings and Other Structures, American Society of Civil Engineers, Reston, Virginia.

Attarnejad, R. and Pirmoz, A. (2014). Nonlinear analysis of damped semi-rigid frames considering moment-shear interaction of connections. International Journal of Mechanical Sciences 81: 165 173.

Azizinamini, A., Bradburn, J.H., Radziminski, J.B. (1987). Initial stiffness of semi-rigid steel beam-to-column joints. Journal of Constructional Steel Research 8: 71-90.

Bathe, K.J. (1996). Finite Element Procedures. Prentice-Hall, New Jersey.

Bernuzzi, C., Zandonini, R., Zanon, P. (1996). Experimental analysis and modelling of semi-rigid steel joints under cyclic reversal loading.Journal of Constructional Steel Research 38(2): 95 123.

Bjorhovde, R., Colson, A., Brozzetti, J. (1990). Classification system for beam-to-column connections. Journal of Structural Engineering 116(11): 3059-3077.

Burden, R.L. and Faires, J.D. (2004). Numerical Analysis, 8th edition, Brooks Cole.

Cabrero, J.M. and Bayo, E. (2005). Development of practical design methods for steel structures with semi-rigid connections. Engineering Structures 27: 1125 1137.

Calado, L. (2003). Non-linear cyclic model of top and seat with web angle for steel beam-to-column connections. Engineering Structures 25: 1189–1197.

Chan, S.L. (1994). Vibration and modal analysis of steel frames with semi-rigid connections. Engineering Structures 16(1): 25-31.

Chan, S.L. and Chui, P.P.T. (2000). Non-linear Static and Cyclic Analysis of Steel Frames with Semi-Rigid Connections. Elsevier, Oxford.

Chan, S.L. and Ho, G.W.M. (1994). Nonlinear vibration analysis of steel frames with semi-rigid connections. Journal of Structural Engineering 120(4): 1075 1087.

Chen, W.F. (2000). Practical Analysis for Semi-rigid Frame Design. Singapore: World Scientific.

Chen, W.F., and Lui, E.M. (1991). Stability Design of Steel Frames. CRC Press, Boca Raton, Florida.

Chen, W.F., Goto, Y., Liew, L.Y.R. (1996). Stability Design of Semi-rigid Frames. John Wiley & Sons Inc., USA.

Chopra, A.K. (1995). Dynamics of Structures, Prentice-Hall, Inc., New Jersey.

Colson, A. (1991). Theoretical modeling of semi-rigid connections behavior. Journal of Constructional Steel Research 19: 213-224.

Cunningham R. (1990). Some aspects of semi-rigid connections in structural steelwork. The Structural Engineer 68(5): 85-92.

Díaz, C., Martí, P., Victoria, M., Querin, O.M. (2011). Review on the modelling of joint behaviour in steel frames. Journal of Constructional Steel Research 67: 741-758.

Eurocode 3. (2005). Design of Steel Structures. Part 1.8: Design of Joints. European Committee for Standardization (CEN) Brussels, Belgium.

Galvão, A.S., Silva, A.R.D., Silveira, R.A.M., Gonçalves, P.B. (2010). Nonlinear dynamic and instability of slender frames with semi-rigid connection. International Journal of Mechanical Sciences 52: 1547 1562.

Ihaddoudène, A.N.T., Saidani, M., Chemrouk, K. (2009). Mechanical model for the analysis of steel frames with semi-rigid joints. Journal of Constructional Steel Research 65: 631-640.

Jones, S.W., Kirby, P.A., Nethercot, D.A. (1980). Effect of semi-rigid connections on steel column strength. Journal of Constructional Steel Research 1: 38 46.

Jones, S.W., Kirby, P.A., Nethercot, D.A. (1983). The analysis of frames with semi-rigid connections – a state-of-the-art report. Journal Construction Steel Research 3(2): 2-13.

Kawashima, S., Fujimoto, T. (1984). Vibration analysis of frames with semi-rigid connections. Computers & Structures 19: 85 92.

King, W.S. (1994) The limit loads of steel semi-rigid frames analyzed with different methods. Computers & Structures 51(5): 475-487.

Kishi, N. and Chen, W.F. (1987a). Moment-rotation Relation of Top and Seat Angle Connections. Structural Engineering Report No. CE-STR-87-4, School of Civil Engineering, Purdue Univ., West Lafayette.

Kishi, N. and Chen, W.F. (1987b). Moment-rotation Relation of Semi-rigid Connections. Structural Engineering Report No. CE-STR-87-29, School of Civil Engineering, Purdue Univ., West Lafayette.

Kishi, N., and Chen, W.F., (1986). Data Base of Steel Beam-to-column Connections. Structural Engineering Report No. CE-STR-93-15, School of Civil Engineering, Purdue Univ., West Lafayette, IN.

Kishi, N., Komuro, M., Chen, W.F. (2004). Four-parameter power model for M–θ curves of end-plate connections. In: ECCS/AISC workshop connections in steel structures V: Innovative steel connections.

Korol, R.M., Ghobarah, A., Osman, A. (1990). Extended end-plate connections under cyclic loading: behavior and design. Journal of Constructional Steel Research 16: 253-280.

Kruger, T.S., Rensburg, B.W.J., Plessis, G.M. (1995). Nonlinear analysis of structural steel frames. Journal of Constructional Steel Research 34: 285-306.

Li, T.Q., Choo, B.S., Nethercot, D.A. (1995). Connection element method for the analysis of semi-rigid frames. Journal of Constructional Steel Research, 32: 143 171.

Lui, E.M. and Chen, W.F. (1986). Analysis and behavior of flexible-jointed frames. Engineering Structures 8(2): 107-118.

Lui, E.M. and Lopes, A. (1997). Dynamic analysis and response of semirigid frames. Engineering Structures, 19(8): 644 654.

Nethercot, D.A., Li, T.Q., Ahmad, B. (1998). Unified classification system for beam-to-column connections. Journal of Constructional Steel Research 45(1): 39-65.

Nguyen, P-C. (2010). Nonlinear Analysis of Planar Semi-Rigid Steel Frames subjected to Earthquakes using Plastic Zone Method. Master Dissertation (in Vietnamese). Hồ Chí Minh, Vietnam.

Nguyen, P-C. and Kim, S-E. (2013). Nonlinear elastic dynamic of space steel frames with semi-rigid connections. International Journal Constructional Steel Research84: 72 81.

Richard, R.M. and Abbott, B.J. (1975). Versatile elastic-plastic stress-strain formula.Journal of the Engineering Mechanics Division 101(4): 511-515.

Sekulovic, M. and Nefovska-Danilovic, M. (2004). Static inelastic analysis of steel frames with flexible connections. Journal of Theoretical and Applied Mechanics 31(2): 101-134.

Sekulovic, M., and Nefovska-Danilovic, M. (2008). Contribution to transient analysis of inelastic steel frames with semi-rigid connections, Engineering Structures 30: 976–989.

Shi, G. and Atluri, S.N. (1989). Static and dynamic analysis of space frames with nonlinear flexible connections. International Journal for Numerical Methods in Engineering 28: 2635-2650.

Shi, G., Shi, Y., Wang, Y. (2007). Behavior of end-plate moment connection under earthquake loading. Engineering Structures, 29: 703-716.

Silva, A.R.D. (2009). Computational System for Static and Dynamic Advanced Analysis of Steel Frames. D.Sc. Dissertation, Graduate Program in Civil Engineering, Federal University of Ouro Preto (UFOP), Ouro Preto/MG, Brazil. (in Portuguese).

Silva, J.G.S., Lima, L.R.O., Vellasco, P.C.G.S., Andrade, S.A.L., Castro, R.A., (2008). Nonlinear dynamic analysis of steel portal frames with semi-rigid connections. Engineering Structures 30: 2566–2579.

Silveira, R.A.M. (1995). Analysis of structural elements slender with unilateral Contact Constraints. Ph.D. Thesis (in Portuguese). Graduate Program in Civil Engineering, PUC-Rio, Rio de Janeiro/RJ, Brazil.

Sophianopoulos, D.S. (2003). The effect of joint flexibility on the free elastic vibration characteristics of steel plane frames. Journal of Constructional Steel Research 59: 995–1008.

Tsai, K.C. Popov, E.P. (1990). Cyclic behavior of end-plate moment connections. Journal of Structural Engineering 116(11): 2917-2930.

Valipour, H.R. and Bradford, M. (2012). An efficient compound-element for potential progressive collapse analysis of steel frames with semi-rigid connections. Finite Elements in Analysis and Design, 60: 35-48.

Vimonsatit, V., Tangaramvong, S., Tin-Loi, F. (2012). Second order elastoplastic analysis of semirigid steel frames under cyclic loading. Engineering Structures 65: 1187-1197.

Vogel, U. (1985). Calibrating Frames, Stahlbau 54: 295-311.

Wong, M.B. and Tin-Loi, F. (1990). Analysis of frames involving geometrical and material nonlinearities, Computer & Structures 34: 641–646.

Xu, Y.L. and Zhang, W.S. (2001). Modal analysis and seismic response of steel frames with connection dampers. Engineering Structures 23 385–396.

Yang, Y.B. and Kuo, S.B. (1994). Theory & Analysis of Nonlinear Framed Structures. Prentice Hall.

Yee, Y.L. and Melchers, R.E. (1986). Moment-rotation curves for bolted connections. Journal of Structural Engineering 112: 615-635.

Zienkiewicz, O.C. and Taylor, R.L. (1991). The Finite Element Method, McGraw-Hill Book Company (UK), vol. 2.

Appendix A

	Algorithm for nonlinear transient analysis
1:	Define the input data: geometric, material and loading properties of the structural system
2:	Obtain the reference nodal load vector, $\boldsymbol{F}_r$ (loading direction)
3:	$t = 0$
4:	$t_1 = t$
5:	Consider the displacement, velocity and acceleration vectors prescribed: $^{t}\mathbf{U}$, $^{t}\dot{\mathbf{U}}$, and $^{t}\ddot{\mathbf{U}}$
6:	Select the time increment Δt
7:	Define the constants: $a_0 = \frac{1}{\beta\Delta t^2};\ a_1 = \frac{\gamma}{\beta\Delta t};\ a_2 = \frac{1}{\beta\Delta t};\ a_3 = \left(\frac{1}{2\beta} - 1\right);\ a_4 = \frac{\gamma}{\beta} - 1;\ a_5 = \frac{\Delta t}{2}\left(\frac{\gamma}{\beta} - 2\right)$ $a_6 = a_0;\ a_7 = -a_2;\ a_8 = -a_3;\ a_9 = \Delta t\left(1-\gamma\right)\ and\ a_{10} = \gamma\Delta t$ where β and γ are the Newmark parameters
8:	**for** eachtime step **do**
9:	$t = t_1$ ▷ Previous time step
10:	$t_1 = t + \Delta t$ ▷ Previous time step
11:	Assemble the matrices: stiffness, $\mathbf{K}$; mass, $\mathbf{M}$; and damping, $\mathbf{C}$
12:	Form the effective stiffness matrix: $\hat{\mathbf{K}} = \mathbf{K} + a_0\mathbf{M} + a_1\mathbf{C}$
13:	Form the effective load vector: $\hat{\mathbf{F}} = {}^{t_1}\lambda\mathbf{F}_r + \mathbf{M}\left(a_2\,{}^{t}\dot{\mathbf{U}} + a_3\,{}^{t}\ddot{\mathbf{U}}\right) + \mathbf{C}\left(a_4\,{}^{t}\dot{\mathbf{U}} + a_5\,{}^{t}\ddot{\mathbf{U}}\right) - {}^{t}\mathbf{F}_i$
14:	Solve for the displacement increment vector $\Delta\mathbf{U}$: $\hat{\mathbf{K}}\Delta\mathbf{U} = \hat{\mathbf{F}}$
15:	**for** k←1, *maximum number of iterations* **do** ▷ ITERATIVE PROCESS
16:	Evaluate the acceleration, velocity and displacement vectors approximations at time t_1 : $^{t_1}\ddot{\mathbf{U}}^{k} = a_0\Delta\mathbf{U}^{k} - a_2\,{}^{t}\dot{\mathbf{U}} - a_3\,{}^{t}\ddot{\mathbf{U}}$; $^{t_1}\dot{\mathbf{U}}^{k} = a_1\Delta\mathbf{U}^{k} - a_4\,{}^{t}\dot{\mathbf{U}} - a_5\,{}^{t}\ddot{\mathbf{U}}$ and $^{t_1}\mathbf{U}^{k} = {}^{t}\mathbf{U} + \Delta\mathbf{U}^{k}$
17:	Update the structure geometry (nodal coordinates)
18:	Evaluate the internal forces vector: $^{t_1}\mathbf{F}_i^{k} = {}^{t}\mathbf{F}_i + \mathbf{K}\Delta\mathbf{U}^{k}$
19:	Evaluate the gradient vector: $^{t_1}\mathbf{R}^{(k+1)} = {}^{t_1}\lambda\mathbf{F}_r - \left(\mathbf{M}\,{}^{t_1}\ddot{\mathbf{U}}^{k} + \mathbf{C}\,{}^{t_1}\dot{\mathbf{U}}^{k} + {}^{t_1}\mathbf{F}_i^{k}\right)$
20:	Solve for the residual displacement vector: $\hat{\mathbf{K}}\delta\mathbf{U}^{(k+1)} = {}^{t_1}\mathbf{R}^{(k+1)}$
21:	Update the incremental displacement vector: $\Delta\mathbf{U}^{(k+1)} = \Delta\mathbf{U}^{k} + \delta\mathbf{U}^{(k+1)}$
22:	**if** $\left\|\Delta\mathbf{U}^{(k+1)}\right\| \Big/ \left\|{}^{t_1}\mathbf{U}^{(k+1)}\right\| \leq tolerance\ factor$ **then**
23:	Exit the iterative processand go to line 26
24:	**end if**
25:	**end for**
26:	Update the acceleration, velocity and displacement vectors at time t_1 : $^{t_1}\ddot{\mathbf{U}}^{(k+1)} = a_0\Delta\mathbf{U}^{(k+1)} - a_2\,{}^{t}\dot{\mathbf{U}} - a_3\,{}^{t}\ddot{\mathbf{U}}$; $^{t_1}\dot{\mathbf{U}}^{(k+1)} = a_1\Delta\mathbf{U}^{(k+1)} - a_4\,{}^{t}\dot{\mathbf{U}} - a_5\,{}^{t}\ddot{\mathbf{U}}$ and $^{t_1}\mathbf{U}^{(k+1)} = {}^{t}\mathbf{U} + \Delta\mathbf{U}^{(k+1)}$
27:	Update the internal force vector at time t_1 :
28:	Update the connections stiffness ▷ See Section 2 and Appendix B
29:	**end for**

Appendix B

	Algorithm for hysteretic behavior of semi-rigid connection
1:	**for** each finite element **do**
2:	Identify the nodal points with semi-rigid connection
3:	**for** each of these nodal points **do**
4:	$M =$ actual moment in this node
5:	$M_{old} =$ moment in this node in the instant t
6:	$\Delta M = M - M_{old}$
7:	**if** $M \cdot M_{old} < 0$ **then**
8:	$\phi_p = \phi_{c:old}$ ▷ See Figures 3 and Appendix A
9:	$i_{Ma} = 0$ and $M_a = 0$ ▷ See Figures 3 and Appendix A
10:	**endif**
11:	**if** $M \cdot \Delta M > 0$ **then** ▷ LOADING PROCESS
12:	$\phi_{c:old} = \phi_c$
13:	Update ϕ_c : $\phi_c = \phi_c + \Delta M \ / \ S_c$
14:	$\Delta\phi_c = \phi_c + \phi_p$
15:	**if** $i_{Ma} = 1$ **then** ▷ Unloading process incomplete
16:	**if** $\left\|M\right\| < \left\|M_a\right\|$ **then**
17:	$S_c = S_{cini}$
18:	**else**
19:	Define the stiffness connection S_c for $\Delta\phi_c$ ▷ See Equations 7, and 4 or 5
20:	$i_{Ma} = 0$ and $M_a = 0$
21:	**end if**
23:	**else if** $i_{Ma} = 0$ **then**
24:	Define the stiffness connection S_c for $\Delta\phi_c$ ▷ See Equations 7, and 4 or 5
25:	**end if**
26:	**else if** $M \cdot \Delta M < 0$ **then** ▷ UNLOADING PROCESS
27:	**if** $M \cdot M_{old} > 0$ and $i_{Ma} = 0$ **then**
28:	$\phi_{ca} = \phi_{c:old}$
29:	$M_a M - \Delta M$ and $i_{Ma} = 1$
30:	**end if**
31:	$\phi_{c:old} = \phi_c$
32:	Update ϕ_c : $\phi_c = \phi_c + \Delta M \ / \ S_c$
33:	$S_c = S_{cini}$
34:	**end if**
35:	**end for**
36:	**end for**